Roman Zettl, BSc

Lithium Ion Conductors based on MIL-121 Metal Organic Frameworks

MASTER'S THESIS

to achieve the university degree of

Diplom-Ingenieur

Master's degree programme: Technical Chemistry

submitted to

Graz University of Technology

Supervisor

Univ.-Prof. Dr.rer.nat. Martin Wilkening
Institute of Chemistry and Technology of Materials

Dr. Ilie Hanzu
Institute of Chemistry and Technology of Materials

Graz, May 2017

AFFIDAVIT

I declare that I have authored this thesis independently, that I have not used other than the declared sources/resources, and that I have explicitly indicated all material which has been quoted either literally or by content from the sources used. The text document uploaded to TUGRAZonline is identical to the present master‘s thesis.

Date

Signature

KURZFASSUNG

In dieser Arbeit wird eine neue, wenig erforschte, Art von Lithium(Li)-Ionenleitern untersucht. MIL-121, ein Metall-organisches Gerüst (MOF = metal organic framework), soll so modifiziert werden, dass es als Festkörperelektrolyt in einer Lithium-Ionen-Batterie zum Einsatz kommen kann. Dafür muss eine ausreichend hohe Li Ionen Leitfähigkeit im Kristallgitter gewährleistet sein. Die Modifizierungen waren einerseits Lithiierung durch Lithiumacetate (LiAc) und Lithiumhydroxid (LiOH) und andererseits Veresterung der Carboxylgruppen von MIL-121 durch Methanol (MeOH), Ethanol (EtOH) und Isopropanol. Darüber hinaus wurde dem Produkt noch eine Flüssigkeit wie zum Beispiel ein Flüssigelektrolyt hinzugefügt, der dazu dienen sollte die Aktivierungsenergie für Li Ionen Sprünge im Kristallgitter zu verringern. Für die veresterten Proben wurde ein Li Salz in den selben Flüssigkeiten gelöst, um Li Ionen in die Struktur einzubringen.

Vorabuntersuchungen zur Überprüfung einer erfolgreichen Modifikation wurden mit ^{1}H magic angle spinning (MAS) Kernspinresonanzspektroskopie (NMR-Spektroskopie) zur Bestätigung der Veresterung und ^{7}Li NMR-Spektroskopie zur Bestätigung der Lithiierung durchgeführt. Es stellte sich heraus, dass beide Reaktionen erfolgreich waren. In weiterer Folge wurden die Pulverproben mit Röntgendiffraktometrie (XRD) untersucht, um die Strukturaufrechterhaltung nach den verschiedenen Modifikationsreaktionen zu untersuchen. Weiters wurde Impedanzspektroskopie durchgeführt, um die Ionenleitfähigkeit zu messen.

Die XRD Messungen ergaben, dass LiAc lithiierte und EtOH veresterte Proben die beste Strukturaufrechterhaltung aufwiesen, wobei bei den anderen Modifikationen eine klare Abweichung der Ausgangsstruktur zu erkennen war. Die Messungen der Ionenleitfähigkeit ergaben einen Trend, der zeigte, dass je höher die Übereinstimmung der modifizierten Struktur mit der Ausgansstruktur war, desto höher auch die Ionenleitfähigkeit. Es zeigten jedoch nur jene Proben, die mit einer ionischen Flüssigkeit ergänzt wurden, eine angemessene Ionenleitfähigkeit. Daraus wurde geschlossen, dass die Li Ionenleitfähigkeit sehr gering war und der Hauptanteil der Ionenleitfähigkeit von Ionen aus der ionischen Flüssigkeit stammt. Eine geringe Li Ionenleitfähigkeit konnte bei einer Probe (Isopropanol verestertes MIL-121, getränkt mit 20 wt% Dimethylcarbonat) bei sehr geringen Frequenzen (0.06 – 1 Hz) beobachtet werden und betrug $\mathbf{2 \cdot 10^{-12}\ S\ cm^{-1}}$.

ABSTRACT

This work was aimed to investigate a new type of solid state lithium (Li) ion conductor as electrolyte for all solid-state Li ion batteries. A metal organic framework (MOF) MIL-121 was modified in two different ways in order to become Li ion conductive. The post synthetic modifications (PSM) were lithiation with lithium acetate (LiAc) and lithium hydroxide (LiOH) as well as esterification of the carboxylic groups of MIL-121 with methanol (MeOH), ethanol (EtOH) and isopropanol. After PSM the porous samples were soaked with different liquids like common liquid electrolytes, which leads to a decreased activation energy of Li ion jumps in the crystal lattice meaning an increased Li ion conductivity of the material. Esterified MIL-121 was soaked with ionic liquids containing lithium bis(trifluoromethane)sulfonimide (LiTFSI), because the introduction of Li ions to the structure was necessary.

Preliminary examination of PSM included ^{1}H magic angle spinning (MAS) nuclear magnetic resonance (NMR) spectroscopy to confirm esterification and ^{7}Li NMR spectroscopy to confirm lithiation. Both reactions were successful. The samples were further investigated by X-ray powder diffraction (XRD) to observe structure maintenance after PSM and impedance spectroscopy (IS) for ionic conductivity measurements.

The XRD measurements showed that LiAc lithiated and EtOH esterified samples showed best maintenance of structure in comparison to the starting material whereas a deviation in structure was clearly observable for the different modified samples. The conductivity measurements showed a trend that, the better the match to the structure of MIL-121 unmodified the better the conductivity of the modified samples. Nevertheless, only samples soaked with an ionic liquid showed conductivities in the order of $\mathbf{10^{-4} - 10^{-6}\ S\ cm^{-1}}$. Small Li ion conductivity was found in one sample (isopropanol esterification modified MIL-121 soaked with 20 wt% of dimethyl carbonate) at very low frequencies (0.06 – 1 Hz) where a conductivity plateau was detectable at $\mathbf{2 \cdot 10^{-12}\ S\ cm^{-1}}$.

VORWORT

Diese Arbeit entstand im Rahmen des Projekts "SOLABAT", das aus Mitteln des Klima- und Energiefonds der FFG (Die Österreichische Forschungsförderungsgesellschaft) gefördert wird. Das Institut für Chemische Technologie von Materialien an der Technischen Universität Graz war zentraler Standpunkt dieser Arbeit, die im Zeitraum von Oktober 2016 bis April 2017 erarbeitet und verfasst wurde.

Neben dem Fördergeber möchte ich mich noch ausdrücklich bei meinem Betreuer Dr. Ilie Hanzu bedanken der mir während dieser Zeit mit Rat und Tat zur Seite stand. Überdies möchte ich Univ.-Prof. Dr. Martin Wilkening für die Möglichkeit danken, die Arbeit in seiner Arbeitsgruppe durchzuführen. Ein großer Dank gilt auch allen anderen Mitarbeitern der Arbeitsgruppe, die für eine immer freundliche und schöne Arbeitsatmosphäre gesorgt haben und auch stets ihre Unterstützung bereitgestellt haben.

Nicht zuletzt möchte ich mich sehr bei meiner Freundin und meiner Familie bedanken, die während der gesamten Studienzeit immer ein offenes Ohr hatten und mir die nötige Motivation gaben.

Graz, 10.5.2017

Roman Zettl

CONTENT

1 Introduction 1

2 Theoretical Aspects 2
2.1 Lithium Ion Batteries 2
2.1.1 Materials 3
2.2 Solid State Electrolytes 4
2.2.1 All-Solid-State Lithium Ion Batteries 5
2.3 Metal Organic Frameworks (MOFs) 6
2.3.1 MOFs as Lithium Ion Conductors 7
2.3.2 MIL-121 and Post-Synthetic Modification Methods 8
2.4 X-ray Powder Diffraction (XRD) 10
2.5 Impedance Spectroscopy (IS) 13

3 Experimental 17
3.1 Synthesis of MIL-121 17
3.2 Esterification of MIL-121 17
3.3 Lithiation of MIL-121 18
3.4 Soaking of MIL-121 18
3.5 X-ray Powder Diffraction (XRD) 19
3.6 Thermogravimetric Analysis (TGA) 20
3.7 Nuclear Magnetic Resonance (NMR) Spectroscopy 20
3.8 Impedance Spectroscopy (IS) 21
3.9 Polarization Experiment 21

4 Results and Discussion 24
4.1 Sodium Hydroxide Titration 24
4.2 X-ray Powder Diffraction (XRD) 25
4.3 Scanning electron microscopy (SEM) 26
4.4 Nuclear Magnetic Resonance (NMR) spectroscopy 27
4.4.1 Liquid ^{1}H NMR 27
4.4.2 Solid State NMR 28
4.4.2.1 ^{7}Li NMR 28
4.4.2.2 ^{1}H MAS NMR 31
4.5 Impedance Spectroscopy (IS) 33
4.6 Polarization Experiment 38

5 Conclusion 41

A. Literature 42
B. Abbreviations 44
C. Appendix 45

1 Introduction

Nowadays, renewable energy resources have significantly gained in importance. However, the main problem of many renewable energy sources is the intermittent character combined with the lack of suitable storage solutions. It is necessary to store high amounts of energy enabling a supply on demand. Therefore, batteries are very important to increase the share of renewable resources in the global energy supply. Peak currents, *e.g.* during the day and in summer (solar cells) or windy periods (wind turbines) have to be stored efficiently so that energy is available, upon request. Therefore, the research in the field of batteries is indispensable to reduce the percentage of energy coming from fossil fuels. A crucial point is the rechargeability of a battery, which means reversibility of the chemical reaction is essential.[1] The lithium ion batteries (LIB) are rechargeable and have been demonstrated to possess the highest energy densities among all available secondary batteries.

Nevertheless, there is the problem of safety and limited voltage window of the currently used liquid electrolytes in LIB. The organic based electrolytes can easily catch fire and undergo oxidative decomposition if a certain voltage is exceeded. This is the reason why extensive research is done in the field of solid state electrolytes which can overcome these obstacles. There are many examples for lithium (Li) ion conductors for solid state electrolytes, but the problem of low ionic conductivity, limiting the power density of the battery is still not solved.

New Li ion conductors could be based on in metal organic frameworks (MOFs). An enormous variety of different MOFs can be synthesized with functional and structural tunability. Together with the properties of thermal stability and porosity MOFs are a promising material for solid state Li ion conductors.

This work aims to synthesize and modify MIL-121, a specific MOF structure, in order to make it Li ion conductive. The conduction could be enhanced through the addition of common liquid electrolytes entering the pores and weaken the bonds between MIL-121 carboxylic groups and Li ions. This is expected to decrease the activation energy of ion jumps in the crystal lattice.

2 Theoretical Aspects

2.1 Lithium Ion Batteries

The Li-Ion Battery (LIB) is a relatively young type of battery and a lot of research is currently done in this field. The element Li first got attention in the 1970's because it is the lightest metal (6.94 g/mol) having the lowest density (0.534 g/cm^3 at 20°C), which is advantageous for applications in portable devices. Furthermore, it shows the highest potential difference vs. standard hydrogen electrode (SHE) with -3.04 V which means it is one of the most electropositive metals. These facts lead to an increased volumetric energy density (in Wh/l) and gravimetric energy density (in Wh/kg) compared to other secondary batteries like lead-acid, Ni-Cd and Ni-MH (*Fig. 1*), which are also available for storage of renewable energy.[2]

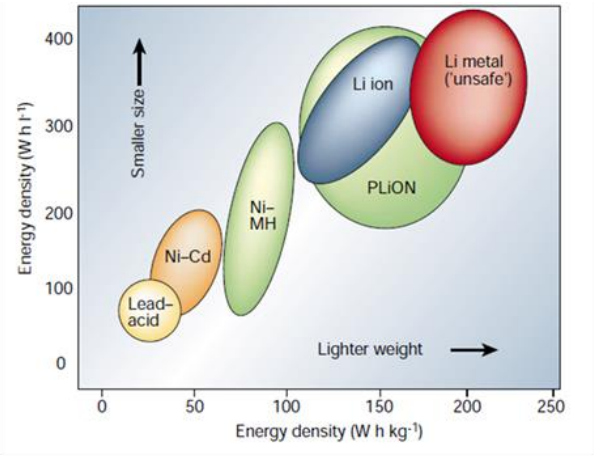

Fig. 1:Comparison of different battery types according to their energy density in Wh/l and Wh/kg [2]
LIB show increased volumetric energy density (in Wh/l) and gravimetric energy density (in Wh/kg) compared to other secondary batteries like lead-acid, Ni-Cd and Ni-MH.

Fig. 2 shows the schematic of a Li-ion battery (b) and in contrast the schematic of a Li-metal battery (a). The main issue with Li-metal batteries is the severe safety problem. With increasing charge/discharge cycles, dendrites are growing on the Li-metal (negative electrode) and are causing short circuit which can lead to explosion.[2] With the Li-ion battery the problem of dendrite growing should be minimized as there is never any metallic lithium in the cell in normal operation conditions.[3]

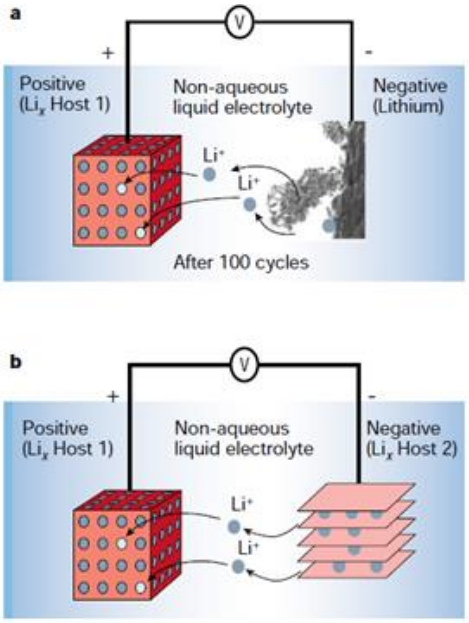

Fig. 2:Schematic of a Li-metal battery (a) and Li-ion battery (b)[2]
With increasing charge/discharge cycles, dendrites are growing on the Li-metal (negative electrode) and are causing short circuit which can lead to explosion.

One drawback of non-metallic Li batteries using Li ions is a lower energy density (*Fig. 1*). Furthermore, LIBs have problems at high temperatures and their cycle life is limited. Until now, large stationary application of LIB for long term storage of renewable energy, do not fulfill the safety criteria as small portable applications do.[4] Over the last decades many materials for cathode, anode and electrolyte were investigated and various approaches were made to minimize the disadvantages of LIB.

2.1.1 Materials

The **negative electrode** material can be either graphite (which can form LiC_6 at full charge), where the insertion of Li^+ ions in the graphite layers is possible, or hard carbon. Graphite has higher specific capacity, lower discharge voltage and lower cost; it is also more sensitive to co-intercalation of electrolytes whereas hard carbon has better rate capability and better low temperature performance. An alternative to those are tin-based oxides or lithium-titanate (LTO).[5]

Positive electrode materials can be classified according to their insertion mechanism:[5]

- olivine type materials (1D, e.g. $LiFePO_4$)
- layered materials (2D, e.g. $LiCoO_2$)
- spinel materials (3D, e.g. $LiMn_2O_4$)

Criteria for good electrode materials are reversibility and electrochemical compatibility with the electrolyte meaning the potential should in principle not exceed the electrolyte potential window, although some deviations are common in practice thanks to some favourable surface chemistry aspects (solid electrolyte interphase, SEI). The redox potential should be high for cathodes and low for anodes. Furthermore, environmental and safety issues play a role and, of course, the costs should be as low as possible.[6] One material capable of acting as both, cathode or anode material, is lithium vanadium phosphate (LVP, $Li_3V_2(PO_4)_3$) which shows Li insertion and extraction in two different potential ranges.[7]

The **electrolyte** should fulfill four main criteria: high ion conductivity, electrochemical stability, wide temperature range of operation and safety features. Liquid electrolytes typically consist of a solvent and a salt. Furthermore, additives might be added. One proven example for electrolytes is $LiPF_6$ as salt and alkyl carbonates (*e.g.* ethylene carbonate, dimethyl carbonate or diethyl carbonate). Mostly the solvent is a mixture of different alkyl carbonates. Alternatives to $LiPF_6$ are $LiAsF_6$, $LiClO_4$, $LiBF_4$, $LiSO_3CF_3$ or $LiN(SO_2CF_3)_2$, but they are either toxic, corrosive, explosive or just too less conductive and, as of today, $LiPF_6$ is the best compromise. One way to improve the performance of the battery through the electrolyte is to use additives which, for example, build protective layers on the electrodes and improve high temperature performance.[4] However, all these liquid electrolytes are a compromise and could never fulfill entirely all the requirements for safety or voltage range for high voltage applications. Therefore, solid state electrolytes are an important way in order to alleviate these problems.

2.2 Solid State Electrolytes

One example where a solid electrolyte is used is the sodium-sulfur-battery (Na/S-battery). The battery consists of two liquid electrodes (Na and S, respectively) separated by a solid electrolyte and is operated at high temperature. The used electrolyte is sodium β-alumina ($NaAl_{11}O_{17}$) which was first investigated in the 1960s when it was found out that sodium β-alumina has a high Na^+ conductivity, which reaches values of liquid electrolytes, albeit at 300 °C. This observation was the beginning of the Na/S battery but also for **solid state ionics**.[8]

Solid state electrolytes (SSE) do not suffer from safety concerns. In contrast to organic based liquid electrolytes, which are highly flammable, they are not supposed to catch fire and have a good stability, which can be thermodynamic or kinetic. The problem of leakage and corrosion is eliminated with solid state electrolyte. Besides, SSE enable high voltage applications. For the usage in cars or as large energy storage devices high voltage is indispensable. Liquid electrolytes have a limited voltage window of 4.3 V (for carbonate based electrolytes). This is however not thermodynamical but kinetic stability. The consequence is an electrolyte decomposition when the cell cycles, which leads to the formation of a so called solid electrolyte interphase (SEI). A low coulombic efficiency and a significantly decreased cycle life are usually associated with a continuous decomposition of the electrolyte. As the technology is always aimed towards better and smaller systems, the issue of miniaturization is also an argument in favour of solid

state electrolytes. With liquid electrolytes a separator has to be used whereas with solid electrolytes thin films can be processed.[9]

Nevertheless, there are drawbacks of SSE. They are limited in their ionic conductivity which has an impact on the power density. The ionic conductivity is related to the resistance of the electrolyte. If the resistance increases (because of lower ionic conductivity) the power and therefore the power density of the cell decreases. A solution to this problem can be, to some extent, thin films of the solid state electrolyte. This will, on the one hand, decrease the volume of the electrolyte (and therefore of the whole cell) and on the other hand decrease the resistance. In addition limited diffusion transport in the electrodes and the larger resistances at electrode/electrolyte interfaces are adverse effects of solid state electrolytes compared to liquid electrolytes, where the liquid is in good contact with the electrodes and therefore these interfacial problems do usually not occur.[9]

The requirements for lithium ion conductors as solid state electrolytes are a high ionic conductivity, because as already mentioned this limits the power density of the battery. Therefore, polycrystalline and ceramic materials used as solid state electrolytes should have insignificant small grain boundaries. Moreover, compatibility with electrodes plays a key role. In addition, the behaviour at different temperatures is important, meaning thermal expansion coefficients have to match. These days the environmental point of view must be considered; the materials must not be either harmful to the environment or toxic. As solid electrolytes will be part of a commercial available application, materials should be cheap as well as easy to produce and process.[10]

2.2.1 All-Solid-State Lithium Ion Batteries

In contrast to the mentioned Na/S battery with liquid electrodes the following chapter focuses on all solid state batteries, meaning it consists of both solid electrodes and electrolytes. Some known and researched examples for Li ion conductors with their ionic conductivity (in S cm^{-1}) are shown below:[11]

- LiPON [12] 2×10^{-6} S cm^{-1}
- Li_2S-based glass [13, 14] 10^{-4}, 10^{-3} S cm^{-1}
- LiSICON-type [15] 3×10^{-3} S cm^{-1}, bulk
- Perovskite-type [16] 2×10^{-5} S cm^{-1}
- Garnet-type [17] 4×10^{-5}S cm^{-1}
- Polymer electrolytes [18] 2×10^{-4} S cm^{-1}

The most promising ionic conductivity shows Li_2S-based glass with up to 10^{-3} S cm^{-1}. This is realized through the addition of a small amount of ortho-oxosalts. The value for LiSICON is given as bulk value, which is always higher than the total ionic conductivity. All conductivities are given at room temperature (RT).[11]

This project focusses on a new field of Li ion conductors. Long et.al. have found Li ion conductivity in two different metal organic frameworks (MOFs) since 2011 and the special properties of MOFs make them interesting for further research in this field.

2.3 Metal Organic Frameworks (MOFs)

Metal organic frameworks (MOFs) are materials which are mainly used in catalysis due to their high porosity. Another application is gas storage, since most MOFs remain stable after removing the solvent, which is a crucial feature for gas catalysis. MOFs consist out of metal containing nodes which are combined through organic linkers. (*Fig. 3*) Common linkers are aromatic carboxylates. With these two main parts of the MOF a variety of different structures can be obtained, which have the opportunity to be tuned via post synthetic modifications (PSM) making it suitable for a certain application. Known researched fields are, as mentioned, catalysis and gas absorption, but it is also applied in sensing.[19] Mechanisms like luminescence, changes in optical properties and the change in electrical properties together with the easy functionalization of the organic linkers are reasons for the application in this field. Examples for sensors are stress-induced chemical detectors, sensors related to changes in optical properties and humidity sensors. [20]

In addition proton[21] and electronic[22] conductivity were found. A contribution to an increased Li ion conductivity was observed by Liu et. al. in 2014 where the water insensitive MOF (MIL-53) stabilized a polymer electrolyte which was sensitive to moisture of air and lead to a tripling in Li ion conductivity. [23]

The property of high thermal stability besides the porosity in combination with the possibility of PSM are interesting features to use MOFs as Li ion conductors for all solid state Li ion batteries. The idea behind this will be explained in the following sections.

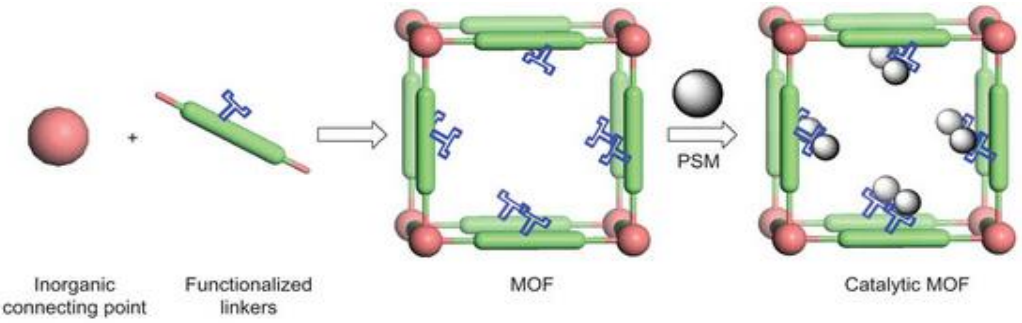

Fig. 3: Schematic illustration of the synthesis and post synthetic modification (PSM) of MOFs
MOFs consist out of metal containing nodes which are combined through organic linkers. Common linkers are aromatic carboxylates. With these two main parts of the MOF a variety of different structures can be obtained, which have the opportunity to be tuned via post synthetic modifications (PSM) making it suitable for a certain application.

2.3.1 MOFs as Lithium Ion Conductors

MOFs as Li ion conductors are a developing field. Only two examples are given in literature from Long et. al. since 2011 who reported Li ion conductivity in two MOF structures after post synthetic modifications.[24,25]

The idea is to modify the MOF in a way that should enable or improve the Li ion conductivity, meaning decrease the activation energy of Li ions jumping from one spot to the other in the crystal lattice. (*Fig. 4*) This is realized with different lithium containing substances as *e.g.* lithium alkoxides, lithium hydroxide or lithium acetate. Furthermore, addition of known liquid electrolytes, solvents for lithium salts and ionic liquids enables ions to move more freely, are attempts to decrease the activation energy (ΔE) for Li^+ jumps through the lattice. This should have the effect that Li ions are "dissolved" in the additionally added liquid, which is assumed to fill the channels, and therefore weaken a bonding to the functional groups of the organic linkers of the MOF. [24, 25]

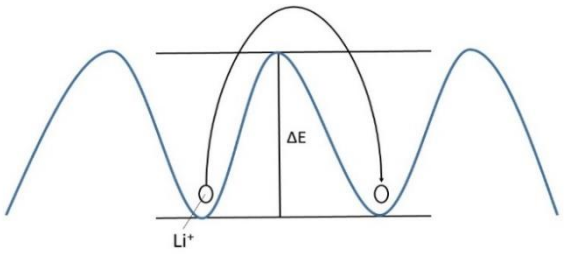

Fig. 4:Energy barrier of a lithium ion moving through a crystal lattice
For Li^+ ion mobility the Li ions have to overcome a certain energy barrier which is aimed to minimize.

Long et. al. used common liquid electrolytes based on carbonate with a Li-salt. Before soaking with this mixture they introduced Li ions to the structure of their magnesium (Mg) based MOF (Mg_2(dobdc); $dobdc^{4-}$ = 1,4-dioxido-2,5-benzenedicarboxylate) by adding lithium alkoxide. The Mg^{2+} binds the alkoxide while the Li can move through the channel freely. They reached a conductivity of 10^{-4} S cm^{-1} at RT. [25]

In 2013 they further investigated the Li ion conduction of a zirconium (Zr) based MOF ($Zr_6O_4(OH)_4(bdc)_6$; bdc^{2-} = 1,4-benzenedicarboxylate) called UiO-66 (Universitetet i Oslo). Here the so called grafting was realized with lithium tert-butoxide (LiOtBu) and resulted in a Li ion conductivity of 1.8 ×10^{-5} S cm^{-1} at RT. [24]

These two encouraging examples were the reason to realize a lithium ion conductor with another promising MOF. In the following the structure of MIL-121 and the idea behind lithium ion movement in MIL-121 is explained.

2.3.2 MIL-121 and Post-Synthetic Modification Methods

MIL-121 (MIL = Matériaux de l′Institut Lavoisier) is an aluminium based MOF ($Al(OH)[H_2btec] \cdot$ (guest), (guest = H_2O, H_4btec = pyromellitic acid). The precursors are $Al(NO_3)_3$ and pyromellitic acid which is an aromatic carboxylate with four carboxylic groups. (*Fig. 5*). Two carboxylic groups are used to link the $AlO_4(OH)_2$ nodes and two of them are available for post synthetic modifications. (*Fig. 6*)

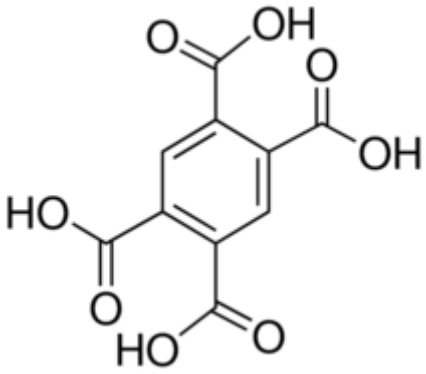

Fig. 5: Structure of pyromellitic acid[26]
The structure includes four carboxylic groups. Two of them serve as a linker to the inorganic metal (Al in case of MIL-121) containing nodes and the remaining two carboxylic groups are available for PSM.

Two different approaches are supposed to modify MIL-121 in a way that leads to Li ion conductivity. First it can be treated with lithium acetate (LiAc) or lithium hydroxide (LiOH). Li^+ binds to the “free” carboxylic groups. After introducing lithium to the structure the solvent has to be removed. Through the addition of small amounts of an ionic liquid (EMIM-TFSI = 1-ethyl-3-methylimidazolium bis(trifluoromethylsulfonyl)imide), diglyme (diethylene glycol dimethyl ether) or tetraglyme (Tetraethylene glycol dimethyl ether), which are known to be good solvents for lithium, the covalent bonds between Li^+ and the carboxylic groups should be weakened and an increase of conductivity should occur.

Moreover, carboxylic groups can be esterified by a Fischer esterification reaction. The aim of this modification is to again weaken the bonding between the moieties and Li^+. Lithium is introduced through ionic liquids (EMIM-TFSI and BMIM-SCN = 1-butyl-3-methylimidazolium thiocyanate) and DMC (dimethyl carbonate), where a lithium salt (LiTFSI = bis(trifluoromethane)sulfonimide lithium salt) is dissolved. In this approach the ions are supposed to move freely through the channels. The path of movement and the channels, respectively are shown in *Fig. 7*. They run along the c-axis, which would be the third dimension in *Fig. 7*. An essential point is to free the pores from the remaining H_2O and pyromellitic acid from the synthesis by thorough washing and drying in vacuum.

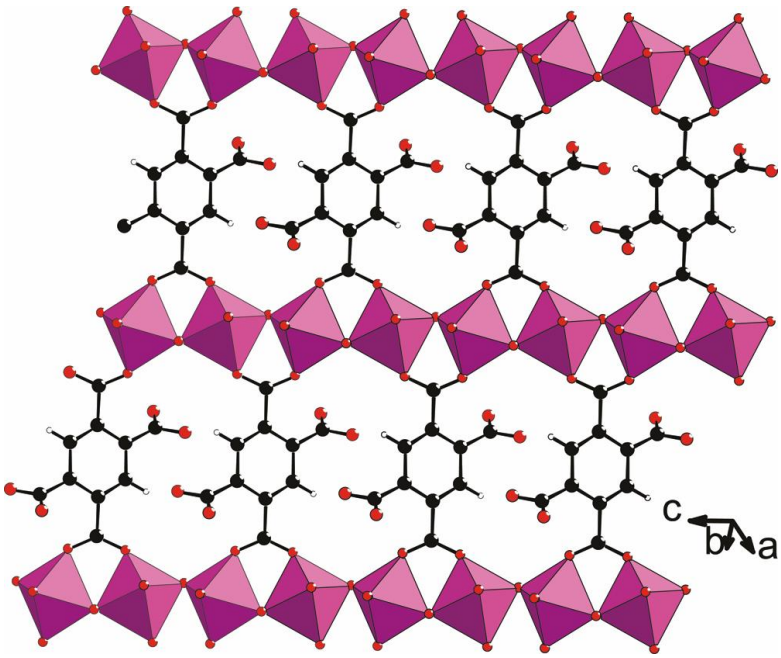

Fig. 6:Structure of MIL-121 showing functionalizable carboxylic groups
Two carboxylic groups are used to link the $AlO_4(OH)_2$ nodes and two of them are available for post synthetic modifications. Purple octahedra symbolize $AlO_4(OH)_2$, black circles carbon, red circles oxygen and open circles hydrogen.

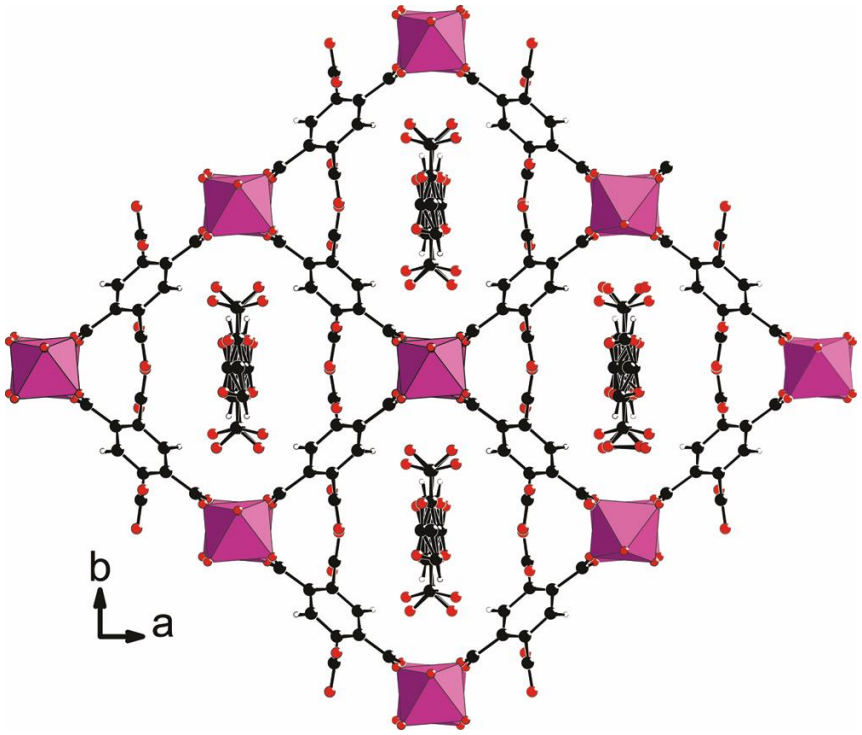

Fig. 7: Structure of MIL-121 showing the possible conduction pathway of ions through the lattice
The conduction pathway of Li ions is expected along the channels which run along the c-axis (would be the third dimension in the figure). An essential point is to free the pores from the remaining H_2O and pyromellitic acid from the synthesis (shown in the the figure inside the pores) by thorough washing and drying in vacuum. Purple octahedra symbolize $AlO_4(OH)_2$, black circles carbon, red circles oxygen and open circles hydrogen.

2.4 X-ray Powder Diffraction (XRD)

This method provides information about the crystal structure of a crystalline material. A broad field of application is the identification of materials or confirmation of synthesis. Moreover, quantitative determination of different phases as well as particle size and crystallization conditions is possible. Concerning the unit cell the following properties and parameters can be determined by XRD: size, symmetry and lattice parameter. Many materials are just available as a powder, but there is also the possibility to analyse a single crystal by single crystal structure analysis.[27]

For a single crystal the exact position of atoms, ions and molecules can be determined by X-rays. Many reflexes are obtained and therefore a high resolution is possible in comparison with powder diffraction.[27]

The X-rays are generated through a setup containing a cathode (hot cathode) and an anode (anti-cathode) inside a high vacuum tube (sealed off tubes). The cathode, which is usually out of tungsten, is heated to 1500 – 2300 °C resulting in electrons emitted from the hot cathode. The electrons are accelerated through applying a high voltage (50 kV). The abrupt stopping of the high energetic electrons at the anode results in specific X-radiation which depends on the anode material (characteristic X-rays) and the applied voltage (bremsstrahlung).[27]

The characteristic X-radiation coming from the X-ray source (XS) passes an optical setup (schematically shown in *Fig. 8* as a filter F in combination with an orifice O). Monochromatic X radiation hits the powder sample (P) and is diffracted at the different atomic planes of the crystal. The diffraction cones have an aperture angle of 2θ. A relation of the wavelength λ of the X-radiation with the distance between crystal planes d and θ is given by the Bragg´s law (1):[27]

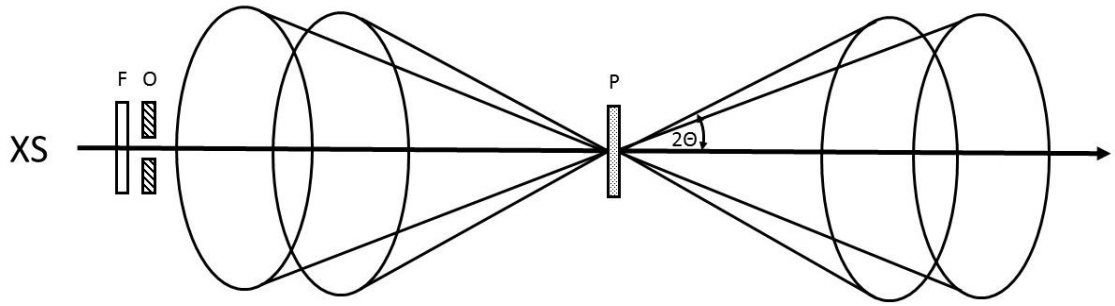

Fig. 8: Schematical pathway of X-rays
Monochromatic X-rays are diffracted at a powder sample (P). The X-rays pass a filter (F) and an orifice (O). The resulting diffraction cone has an angle of 2θ. XS is the X-ray source.[27]

$$n \cdot \lambda = 2 \cdot d \cdot \sin\theta \qquad \textbf{(1)}$$

Fig. 9 is a schematic representation of Bragg´s law. The green dots are lattice points or atoms, respectively. The incident beam hits the crystal in an angle of θ and is reflected in the same angle.

The following techniques are used to evaluate the X-radiation for powders. The Debye-Scherrer camera and the Straumanis procedure are examples for camera techniques. Alternatively, so called diffractometers are applied which use a scintillator counter (Bragg–Brentano-Diffractometer). With the scintillator counter the X-ray photons are in further consequence transformed in electric signals that can be counted and processed.[27]

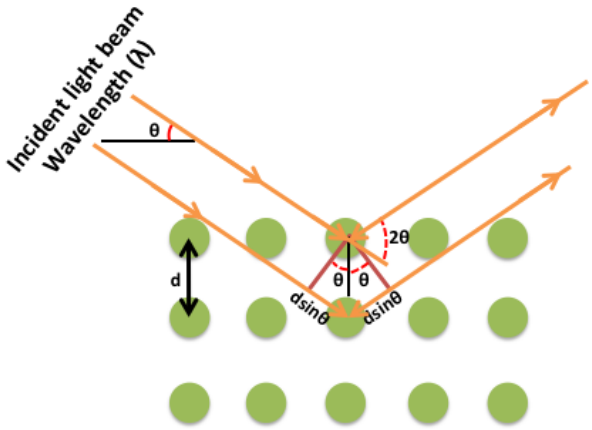

Fig. 9: Bragg´s law schematically described
The green dots are lattice points or atoms, respectively. The incident beam hits the crystal in an angle of θ and is reflected in the same angle. d symbolizes the distance between crystal planes and θ is the angle between incident beam and scattered beam.[28]

In a final procedure the data is further processed by the Rietveld refinement. Through the least square method, the measured data is adjusted to a theoretical line profile which is obtained through a structure model. This structure model can be calculated from preliminary parameters of the XRD measurement.[27]

Three distinct information can be obtained. First there is the diffraction angle 2θ. It depends on the size and symmetry of the unit cell whereby the parameter d (distance between crystal planes) can be determined. Furthermore, the intensity is related to the type and arrangement of the atoms in the crystal lattice. By crystal structure analysis one can get information about three dimensional (3D) arrangement of atoms or molecules in the material. Third, there is a relation between particle size and the condition of crystallization and the shape of the line of diffraction interferences.[27]

Fig. 10 shows, as an example, a X-ray diffractogram of MIL-121 with 2θ on the abscise and the normalized intensity (here written as counts) on the ordinate. In this work XRD will mainly be used to confirm the structure of the material and compare it after different post synthetic modifications.

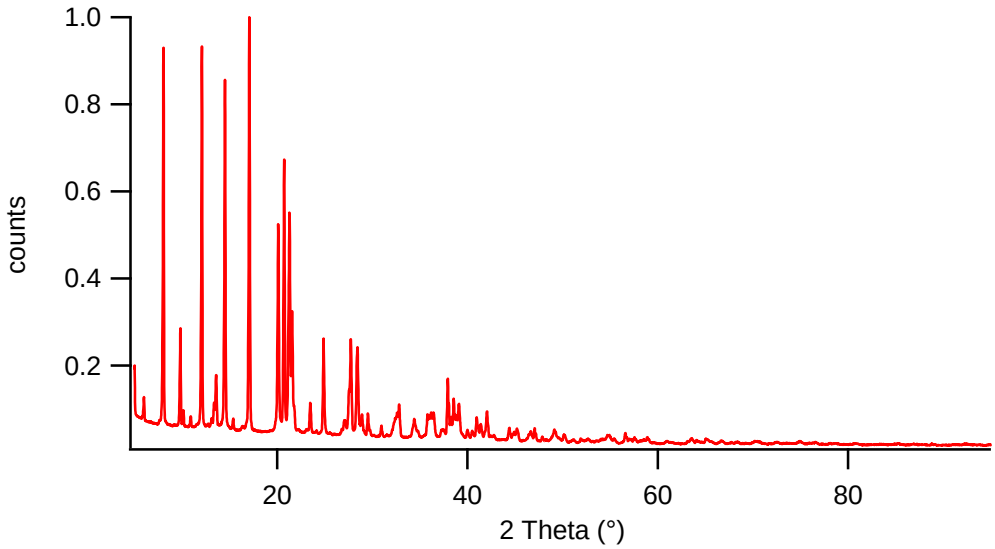

Fig. 10: X-ray diffractogram of MIL-121

2.5 Impedance Spectroscopy (IS)

Impedance spectroscopy is used to determine the ionic conductivity. The technique enables analysis of diffusion of ions in solids. In principle an alternating voltage u(t) is applied to a sample (usually pressed to a pellet with thickness d and surface area A) and the answering current I(t) is measured. (*Fig. 11*, *Fig. 12*) A phase shift Φ between u(t) and I(t) occurs when the material of interest is dielectric, meaning an insulating material that can be polarized. As a result, the frequency and temperature dependent conductivity is obtained. The frequency window of the experiment ranges from mHz to GHz.[29]

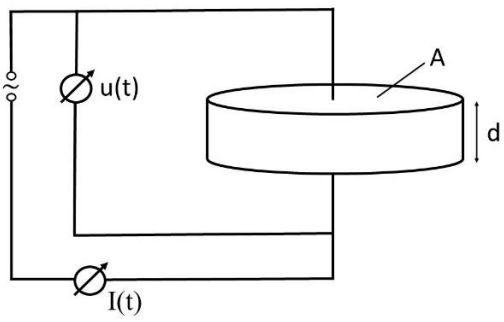

Fig. 11: Schematic of an impedance measurement setup
u(t) and I(t) symbolize the applied voltage and the measured current, respectively. A is the surface area of the pellet and d the thickness of the pellet.[29]

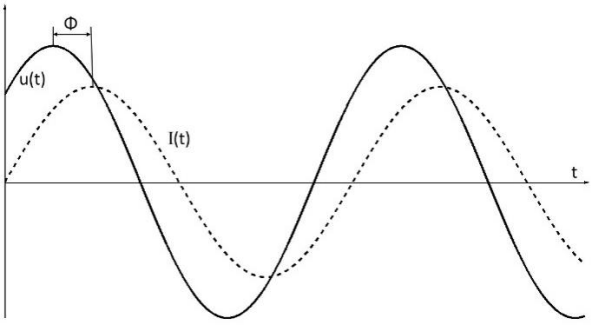

Fig. 12: Sinusoidal u(t)- and I(t)-curve with phase shift Φ[29]

Fig. 13 shows the ionic conductivity (σ) as a function of frequency (ω = radial frequency, ω = 2 π f; f = frequency). Furthermore, corresponding energy diagrams for ions diffusing through a crystal lattice are shown. Ions are located in potential energy wells and have to overcome a certain energy barrier to jump to the next well, which is then understood as ion diffusion in the solid. The higher the energy barrier, the more difficult it is to overcome the barrier and the lower the ionic conductivity.[30]

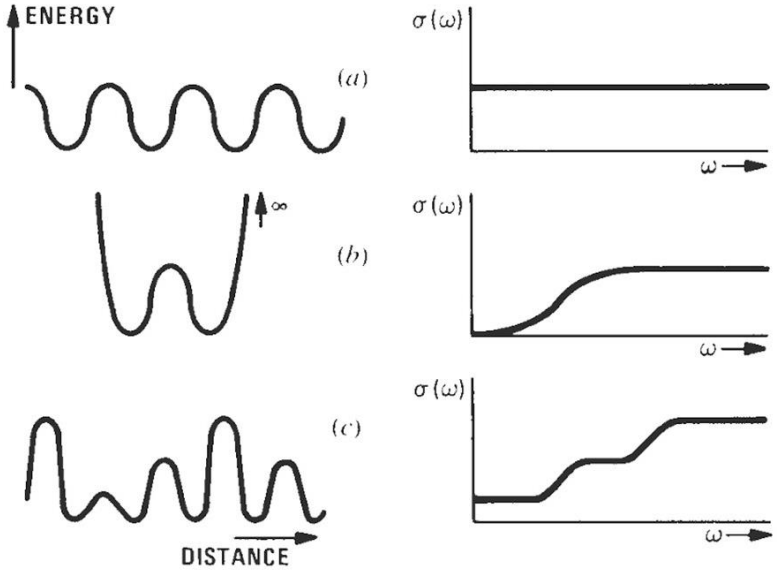

Fig. 13: Conductivity isotherms of different energy profiles [30]
Different energy profiles are possible for an ion when moving through a solid: a) constant periodic activation energy, b) two energy wells, c) various activation energies possible (*e.g.* in the bulk or at grain boundaries of a polycrystalline material). σ(ω) symbolized the conductivity as function of the frequency in S cm^{-1} and ω the frequency in Hz.

For an *e.g.* polycrystalline solid state electrolyte one would expect two plateaus: one for bulk conductivity (higher conductivity plateau; $\sigma_{DC'}$) and one for conductivity through the grain boundaries (lower conductivity plateau; σ_{DC}). At low frequencies electrode polarization occurs resulting in a drop of conductivity. (*Fig. 14*) With σ_{DC} a diffusion coefficient can be calculated from (2):

$$D_\sigma = \frac{\sigma_{DC} \cdot k_B \cdot T}{N \cdot q^2} \qquad \textbf{(2)}$$

D_σ is the diffusion coefficient obtained from IS, σ_{DC} is the value of the conductivity isotherm, where $\sigma \neq f(\omega)$ (lower conductivity plateau), k_B is the Boltzmann constant ($1.38 \cdot 10^{-23}$ m^2 kg s^{-2} K^{-1}), T is the temperature in Kelvin, N is the number of charge carriers per Volume (charge carrier density) and q is the charge of a particle. σ_{DC} is also used to compare different ion conductors with each other at a certain temperature. The capacities in the depicted areas (b, g.b., e) are: bulk: C < 10 pF, grain boundary: C > 100 pF and electrode: C >> 100 pF.

The areas where $\sigma = f(\omega)$ can be fitted through the so called Jonscher ansatz (3), where n can attain values from 0.6 – 1.0:

$$\sigma \propto \sigma_{DC} + A \cdot \omega^n \qquad \textbf{(3)}$$

σ_{DC} is the frequency independent conductivity and A is a constant.

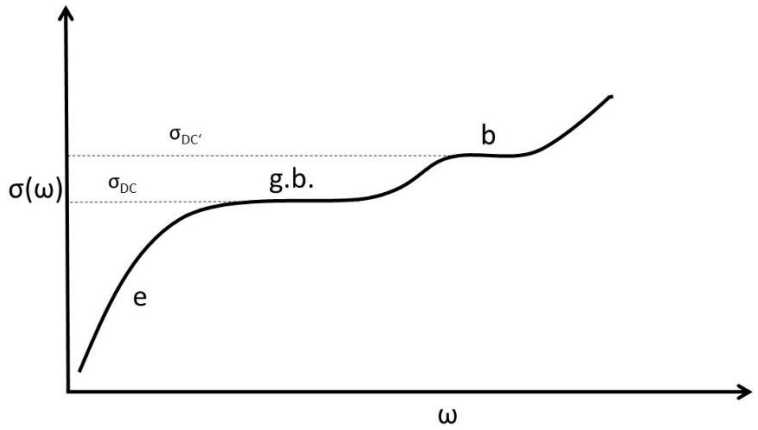

Fig. 14: Conductivity isotherms of a solid state electrolyte
For an *e.g.* polycrystalline solid state electrolyte one would expect two plateaus: one for bulk conductivity (b, higher conductivity plateau; $\sigma_{DC'}$) and one for conductivity through the grain boundaries (g.b., lower conductivity plateau; σ_{DC}). At low frequencies electrode polarization (e) occurs resulting in a drop of conductivity. $\sigma(\omega)$ symbolized the conductivity as function of the frequency in S cm^{-1} and ω the frequency in Hz whereas σ_{DC} is the value of the conductivity independent of the frequency.

Another way to demonstrate the measurement results of impedance spectroscopy is by using the so called Nyquist plot. The real impedance is plotted against the imaginary part of the impedance. (*Fig. 15*) Again three areas can be distinguished: bulk, grain boundary and electrode. A complete half circle can be shown with electric components as a parallel circuit of an ohmic resistance and a capacitor. The frequency increases from right to left.[31]

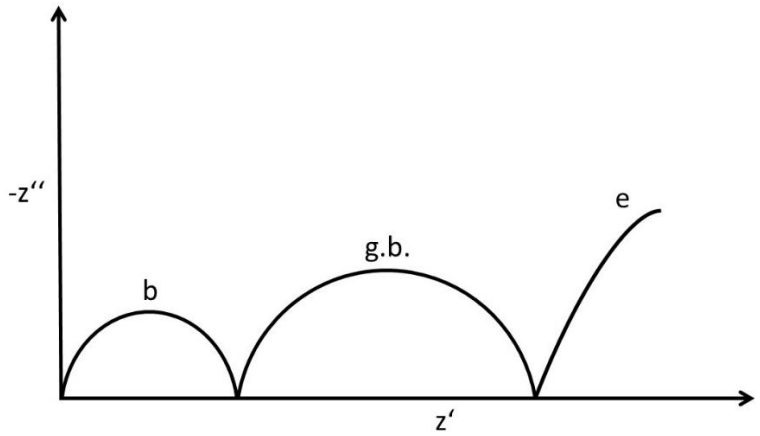

Fig. 15: complex impedance plot (Nyquist plot) [31]
Three areas can be distinguished: bulk (b), grain boundary (g.b.) and electrode (e). A complete half circle can be shown with electric components as a parallel circuit of an ohmic resistance and a capacitor. The frequency increases from right to left. z' symbolized the real impedance in Ω and -z'' the complex impedance in Ω.

3 Experimental

3.1 Synthesis of MIL-121

MIL-121 was synthesized by a hydrothermal synthesis. A Teflon beaker with a volume of 250 mL was filled with aluminium nitrate nonahydrate ($Al(NO_3)_3 \cdot 9\ H_2O$), pyromellitic acid (H_4btec = 1,2,4,5-Benzenetetracarboxylic acid) and an appropriate volume of deionized water. (~50 mL) The beaker was put into a stainless steel autoclave (*Fig. 16*) and stirred for a few minutes. The autoclave was closed and a temperature sensor was connected to check the temperature program of the control unit. The reaction was realized for 24 h at 210 °C using a heating rate of 4 °C/min.

Fig. 16: Stainless steel autoclave for hydrothermal synthesis

The product was a white solid which was sedimented at the bottom with a clear yellow liquid above. The product was centrifuged and washed with deionized water several times and put in an oven at 80 °C to dry. Finally, MIL-121 was characterized by XRD.[32]

3.2 Esterification of MIL-121

In order to modify the samples to get the desired Li ion conductivity an esterification was realized due to mentioned reasons in section *2.3 Metal Organic Frameworks (MOFs)*. The procedure was done following a common Fischer esterification, where sulphuric acid is used as a catalyst. The idea was to esterify the two free carboxylic groups of the MIL-121 structure with the following alcohols: ethanol, methanol and isopropanol. Since this type of esterification had not been done before, the reaction time was unknown and set to one week, because this heterogeneous reaction in the pores was expected to need time. The reaction mixture was a heterogeneous white suspension. During the reaction the evaporated alcohol was liquefied through a reflux condenser and passed through zeolite molecular sieves in order to obtain a water free material. The product *MIL-121_est* was washed with the corresponding alcohol and dried at 80 °C. *MIL-121_est* was analysed in order to observe if the structure was maintained by XRD and if the esterification was successful by solid state proton NMR with Magic Angle Spinning (MAS).

Furthermore, the precursor pyromellitic acid was esterified. This esterification was carried three times with three alcohols (methanol, ethanol, isopropanol) and for one day. This was done to confirm if esterification of pyromellitic acid in principle works and to obtain some reference spectra. The confirmation was done by liquid ^{1}H NMR.

3.3 Lithiation of MIL-121

A second approach of modification was to lithiate MIL-121. The starting material is exposed to a 1 M solution of lithium acetate (LiAc) and stirred for one day. Lithium hydroxide (LiOH) was additionally used for lithiation in the same way in a first approach. Preliminary XRD measurements showed that the structure was destroyed and therefore the following three different measurement setups were chosen:

- same setup as it was realized with LiAc
- adding a 0.5 M solution of LiOH in steps (titration) in order to have milder reaction conditions regarding the pH value to protect the structure against destruction (total volume added: 29.0 mL)
- realize the titration method with more volume (35.5 mL) to guarantee complete lithiation (not further investigated)

The resulting *MIL-121_Li* was centrifuged and washed with deionized water and dried at 80 °C. Analysis with XRD was realized to confirm the structure maintenance. The confirmation of lithiation was realized by ^{7}Li NMR and conductivity measurements were carried out after sample preparation for those two measurement techniques.

In order to confirm if the titration method works, the same experiment was carried out with sodium hydroxide (NaOH) instead of LiOH. For this preliminary experiment small amounts of sample were taken and afterwards the presence of Na in the structure was confirmed by energy-dispersive X-ray spectroscopy (EDX) and structure maintenance was confirmed by XRD.

3.4 Soaking of MIL-121

Before the different modified MIL-121s were soaked they were dried at high vacuum ($\sim 10^{-6}$ mbar) at temperatures from 165 – 280 °C. These temperatures were obtained through TGA (thermo gravimetric analysis) and realized in a helium flow atmosphere and a heating rate of 1 °C/min.

The soaking was carried out in a glove box with argon (Ar) atmosphere. The amounts of liquid added to the different modified MIL-121s were calculated through the density of the liquid. 10, 20, 30 and 40 wt% were added and thoroughly mixed with a spatula until a material with a homogenous colour remains. Afterwards the soaked samples were but into a borosilicate bottle which was supposed to be air tight and put into an oven at 60 °C in order to reach a higher degree of homogeneity. After drying the samples were transferred back to an Ar glove box in order to minimize contact with air. In Tab. 1 the liquids for soaking are tabulated. Esterified samples were soaked with liquids which had LiTFSI dissolved in different concentrations. The solubilities were taken from Gross *et. al.*[33].

Tab. 1: Liquids for soaking
Liquids for MIL-121_est have LiTFSI dissolved in different concentrations

MIL-121_Li	**MIL-121_est**
EMIM-TFSI	0.4 M LiTFSI in EMIM-TFSI
Diglyme	1.3 M LiTFSI in BMIM-SCN
Tetraglyme	1.0 M LiTFSI in DMC

EMIM-TFSI (18 ppm from iolitec) and anhydrous diglyme and DMC (Sigma Aldrich) were used as they were delivered from the suppliers. The other liquids as well as the LiTFSI salt were dried before use. BMIM-SCN was dried in an open glass vial placed in a borosilicate screw-cap bottle (Schott) with metallic Li placed aside the open vial containing the ionic liquid. The closed borosilicate glass bottle was kept at 60 °C in an oven for one week resulting in 40 ppm water content measured by a Karl Fischer (KF) titration. Tetraglyme was dried with zeolite molecular sieves in the common way leading to 38 ppm (KF) water content. LiTFSI was dried under vacuum (10^{-3} mbar) at 140 °C over night.

3.5 X-ray Powder Diffraction (XRD)

The X-ray powder diffraction measurements were realized with a Bruker D8-Advance X-ray powder diffractometer and a Lynxeye detector. The radiation was Cu-Kα and angles from 10 - 100° 2θ with a step size of 0.02° 2θ were measured. Depending on the measurement the duration per step was 2 – 4 s.

3.6 Thermogravimetric Analysis (TGA)

TGA measurements were carried out in order to determine the drying temperature for the modified samples. The resulting graphs of the measurements are shown in the appendix. The parameters of the measurement were a rate of 1 °C/min in helium atmosphere. The temperature range was RT – 550 °C. The measurements were realized with a STA (simultaneous thermal analysis)-device from Netzsch (STA 449 C) coupled with a mass spectrometer QMS 403 C (Netzsch). This analysis method connects two methods, differential scanning calorimetry (DSC) and TGA.

3.7 Nuclear Magnetic Resonance (NMR) Spectroscopy

The soaked samples with a wt% of 30 as well as the LiOH and LiAc samples without soaking were measured with NMR spectroscopy. Approximately 20 mg of sample were filled in an NMR tube, embedded between two separators (Whatman filter paper, Ø = 1 cm) and pressed together by a hard copper wire inside an Ar glove box. The tube is equipped with a ground joint and sealed with a valve. A vacuum (10^{-3} mbar) is applied outside the glovebox and the tube is melted with a flame (natural gas and oxygen). This preparation referred to the static ^{7}Li NMR experiments which were carried out with a Brucker Avance III 300 spectrometer with a 7 Tesla cryomagnet. This corresponds to a resonance frequency of 116.59 MHz for ^{7}Li. A ceramic probehead, a HZ03347 PH HPBBHT Insert 33P F high Q capacitor as well as a 70 – 125 MHz filter were used.

For MAS measurements rotors with a diameter of 2.5 mm were filled. Some of the pure ester samples had to be diluted with Al_2O_3 due to their low melting point. The Al_2O_3 has the role to immobilize the (possibly) molten compound. In order to confirm esterification this proton NMR was realized for the following samples: esterified MIL-121, esterified pyromellitic acid and original MIL-121. The ^{1}H MAS measurements were carried out with a Bruker Avance III 500 spectrometer and a 11 Tesla cryomagnet (giving a resonance frequency of 500 MHz for ^{1}H). A MAS probehead with 2.5 mm rotors and a spin rate of 30 KHz was used.

For liquid NMR pyromellitic acid and the three esterified pyromellitic acid samples were dissolved in deuterated solvents (chloroform and acetone) and measured at room temperature and a pulse angle of 30 °. The spectrometer was a Unity Inova 500 MHz NB High Resolution FT NMR (Nuclear Magnetic Resonance Spectrometer) from Varian with the following probes:

- $^{1}H\{^{15}N\text{-}^{31}P\}$ 5 mm PFG indirect detection probe
- $^{1}H\text{-}^{19}F$ / $^{15}N\text{-}^{31}P$ 5 mm switchable probe

3.8 Impedance Spectroscopy (IS)

After soaking, the samples are pressed to pellets (*Fig. 17*) in an Ar glove box. A load of 0.3 tons was applied with a press of 5 mm in diameter for 3 minutes. The thickness of the pellet was measured, too and varied from 0.5 – 1.3 mm. Afterwards the pellets were transferred into a mask for physical vapour deposition which was carried out at 10^{-5} mbar. Gold was evaporated until a layer thickness of 80 nm was reached. (*Fig. 18*) At the end the pellet was assembled in a coin cell in order to protect the samples from the atmosphere during impedance measurements.

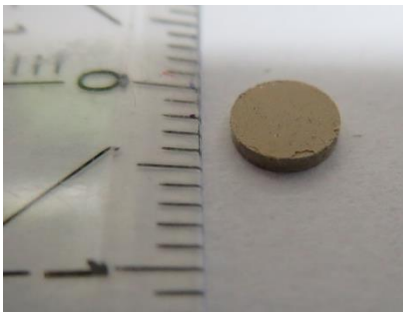

Fig. 17: Pressed pellet before Gold coating

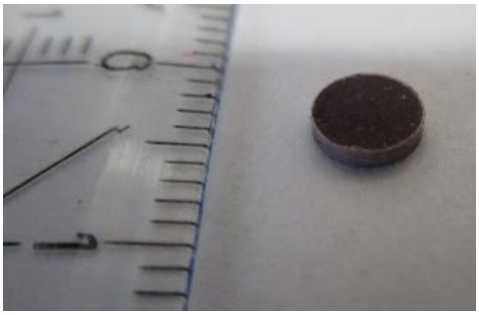

Fig. 18: Pressed pellet after Gold coating

The measurements were carried out by a Concept 80 system (Novocontrol) with an Alpha-A RF impedance analyser and an active ZGS sample cell. Single-sweep measurements at room temperature were done with frequencies from 10 MHz to 10 mHz.

3.9 Polarization Experiment

In order to determine the transport number of Li^{+} through the Bruce Vincent method (4) a polarization experiment was carried out.[34] I_{SS} is the current at steady state and I_0 is the initial current. The requirement is a known impedance, which is measured before and after the polarization experiment.

$$T_{Li^+} = \frac{I_{SS}}{I_0} \quad \textbf{(4)}$$

MIL-121 was not easy pressable and therefore a special setup (Fig. 19) had to be built in order to allow the measurement of a composite pellet. The measurement was realized with an insulating press die and the pressure (0.3 tons, Ø = 5 mm) was applied during the experiment. The different powders were added to a laboratory made press set out of a polymer. The top and the bottom of the press set were separate parts in form of flat cylinders. The pellet was pressed between two cylindrical steel parts. A copper foil was placed between the cylindrical metal parts and the insulating end parts of the press set. With this schematic the press itself is not connected to the metal parts of the press set whereas the pellet could be connected to a potentiostat via the copper foils and the metallic cylinders. The composite pellet was composed of the following layers in the following order:

- Copper powder (negative current collector)
- VS_2[a](including approx. 20 wt% MIL-121_Li; LiAc treated, soaked with 30 wt% EMIM-TFSI); negative electrode
- MIL-121_Li (LiAc treated, soaked with 30 wt% EMIM-TFSI); electrolyte
- LVP/C[b] (including approx. 20 wt% MIL-121_Li; LiAc treated, soaked with 30 wt% EMIM-TFSI); positive electrode
- Aluminium powder (positive current collector)

[a]Vanadium disulfide
[b] Lithium vanadium phosphate ($Li_3V_2(PO_4)_3$) was carbonized through a sol-gel synthesis (citric acid is the gelating agent and the carbon source).

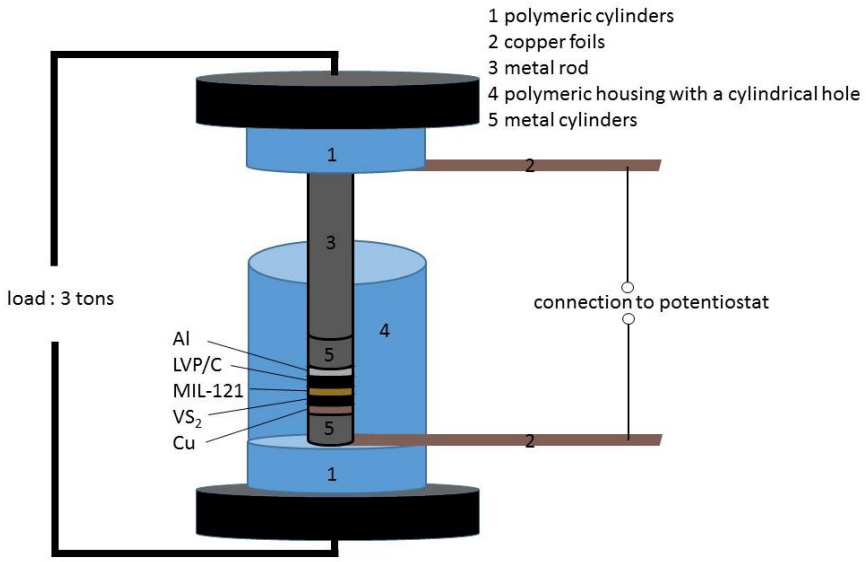

Fig. 19: Schematic of the setup for the polarization experiment and associated measurements (GCPL, IS)

Detailed description of pellet components see list above.

By using vacuum grease the press set was sealed and transferred from the Ar glovebox to the measurement device. The device was a BioLogic VMP3 potentiostat which is a research-grade multi-channel potentiostat controlled by EC-Lab software. For the impedance measurements a frequency range of 500 kHz to 50 mHz and a sinus voltage amplitude of 10 mV were set. The polarization was carried out by applying 30 mV for 12 h.

Previous to that the cell was cycled to reach a steady state. This was done with a Bio-Logic MPG2 potentiostat which is a research-grade multi-channel potentiostat controlled by EC-Lab software. Positive and negative currents of 8, 16 and 32 µA are alternatingly applied in a voltage range of 0.2 – 1.6 V. This is equivalent with charging and discharging the cell.

4 Results and Discussion

4.1 Sodium Hydroxide Titration

In order to confirm that the titration of LiOH works a similar experiment was performed with NaOH. These preliminary experiments included XRD to confirm structure maintenance and EDX to confirm Na in the structure.

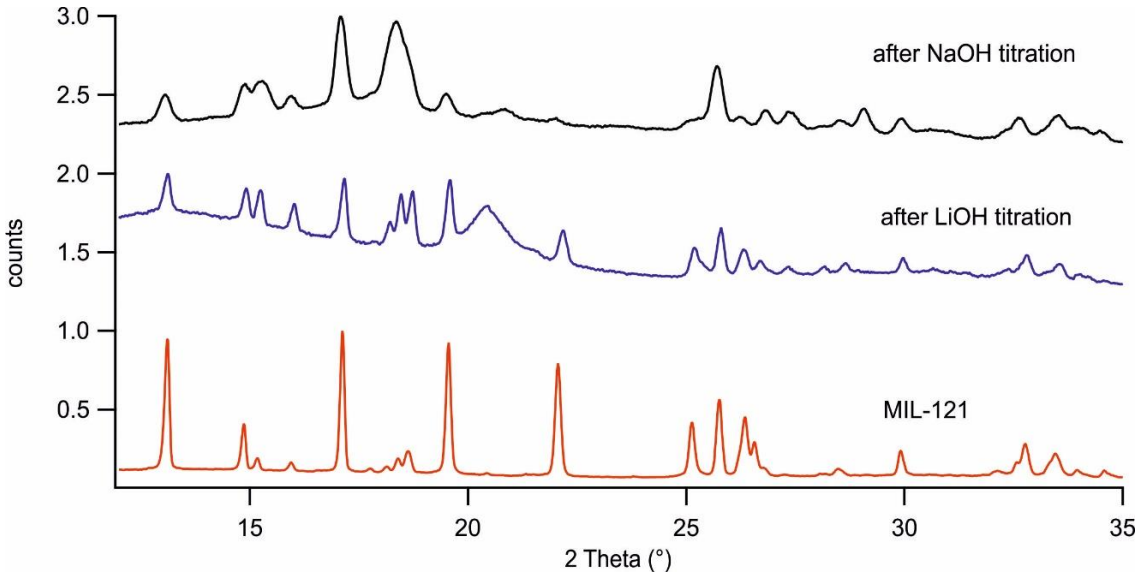

Fig. 20: X-ray diffractogram of MIL-121 preliminary titration experiments (type of modification written above the curve) in comparison to each other and the original MIL-121 structure
Both experiments lead to a certain deviation from the original structure but a structure maintenance could be obtained to some extent. These similarities in structure compared to the original MIL-121 lead to the application of this experimental setup to a larger amount of sample.

Fig. 20 shows that both experiments lead to a certain deviation from the original structure but a structure maintenance could be obtained to some extent. These similarities in structure compared to the original MIL-121 lead to the application of this experimental setup to a larger amount of sample. Moreover, Na could be confirmed by EDX meaning also Li could bind to the carboxylic groups of MIL-121. This measurement served also as reference point for the static solid state ^{7}Li NMR where Li should be found in the structure. It still cannot replace the ^{7}Li NMR measurement, because light elements like Li cannot be seen with EDX.

4.2 X-ray Powder Diffraction (XRD)

Fig. 21 shows the X-ray diffractograms of MIL-121 at the bottom in red. Furthermore, different modification attempts were analysed and are shown in the upper part. LiAc (green) revealed the best match to the original structure which can be seen when position and intensity of the reflexes are compared. The LiOH treatment did not work in a first attempt shown in black. It seems that the high pH value of the 1M LiOH solution destroyed the structure. Further experiments where LiOH was added in steps (titration) were more successful. The addition of more volume (35.5 mL), shown in orange, lead to a larger deviation from the original structure than the titration attempt with 29 mL (blue). Nevertheless, the blue curve deviates a lot from what should be obtained (red), not only in the intensity of reflexes but also in the position. Some of the reflexes had the same position (*e.g.* at 17 and 19 ° 2θ), but additional reflexes occur (*e.g.* 16 and 18° 2θ). Lithiation by titration with LiOH could be carried out with even less volume to obtain a better match with the original structure including a risk of no complete lithiation of MIL-121. LiAc is not only the easier modification method it but leads additionally to a better match in XRD diffractograms with the pure MIL-121 structure unmodified, meaning the best structure maintenance was revealed with the LiAc treatment.

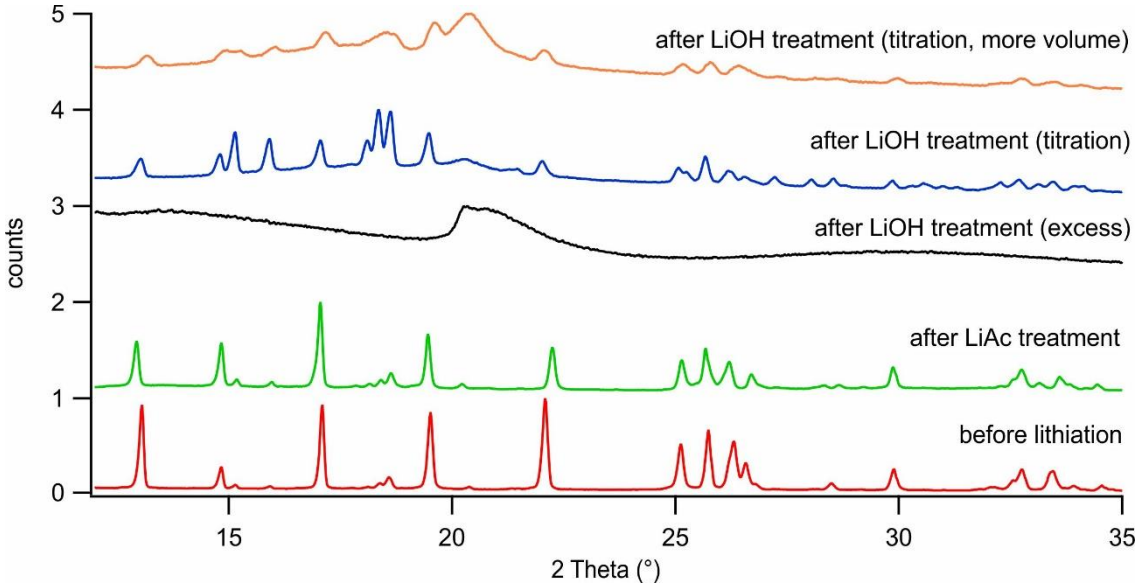

Fig. 21: X-ray diffractogram of modified MIL-121 (type of modification written above the curve) in comparison to each other and the original MIL-121 structure
LiAc (green) revealed the best match to the original structure which can be seen when position and intensity of the reflexes are compared. The LiOH treatment did not work in a first attempt shown in black. It seems that the high pH value of the 1M LiOH solution destroyed the structure. Further experiments where LiOH was added in steps (titration) were more successful. The addition of more volume, shown in orange, lead to a larger deviation from the original structure than the titration attempt with less volume (blue). Nevertheless, the blue curve deviates a lot from what should be obtained (red), not only in the intensity of reflexes but also in the position.

Fig. 22 shows the X-ray diffractograms of MIL-121 at the bottom in red. Furthermore, different esterification attempts were analysed and are shown above. Ethanol esterification (green) revealed the best match to the original structure. Methanol esterification (blue) on the first view seemed to be in a good agreement with the original structure but shows differences in intensities. In orange the diffractogram of the isopropanol esterification is shown and in the area of 22 to 25 ° 2θ additional reflexes occur. The preferred modified sample is therefore the EtOH-ester concerning structure maintenance.

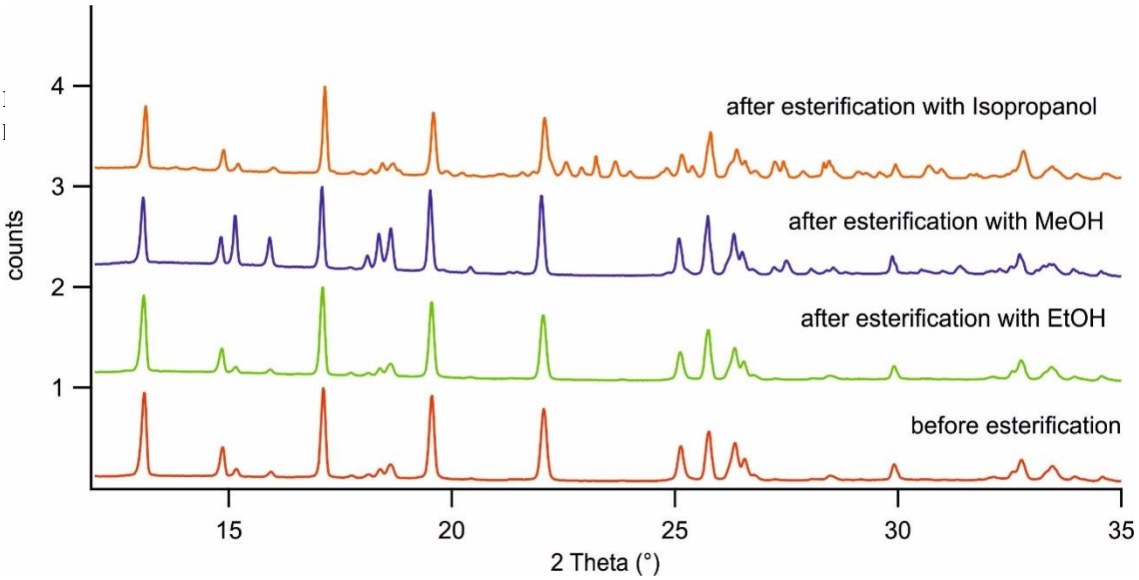

Fig. 22: X-ray diffractogram of esterified MIL-121 (used alcohol written above the curve) in comparison to each other and the original MIL-121 structure
Ethanol esterification (green) revealed the best match to the original structure. Methanol esterification (blue) on the first view seemed to be in a good agreement with the original structure but shows differences in intensities. In orange the diffractogram of the isopropanol esterification shows additional reflexes in the area of 22 to 25 ° 2θ. The preferred modified sample is therefore the EtOH-ester concerning structure maintenance.

4.3 Scanning electron microscopy (SEM)

In order to see how the structure of the MOF changed with the modifications SEM images were recorded and compared to each other. Below SEM images with a magnification of 2500x are shown.

It can be clearly seen from *Fig. 24* - *Fig. 27* that LiAc lithiation (*Fig. 26*) and the esterification (ethanol esterification exemplary shown in *Fig. 27*) showed a structure comparable to the original structure of the pure MIL-121 without any modification (*Fig. 24*) in the SEM images. This was not the case for the LiOH treated MIL-121 where the structure was destroyed and crystallinity cannot be observed anymore. Therefore, a titration technique, where LiOH was just added in steps had to be applied. Other SEM images can be found in the appendix.

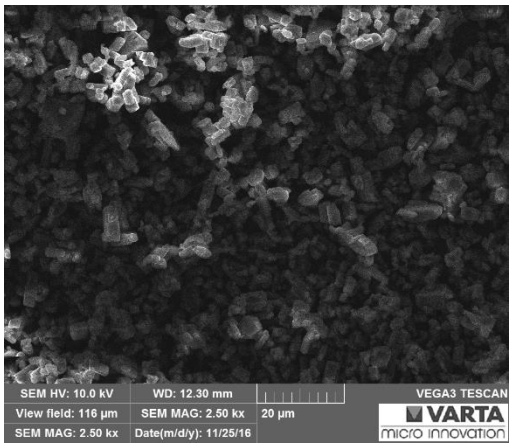

Fig. 24: SEM image before modification (pure MIL-121)

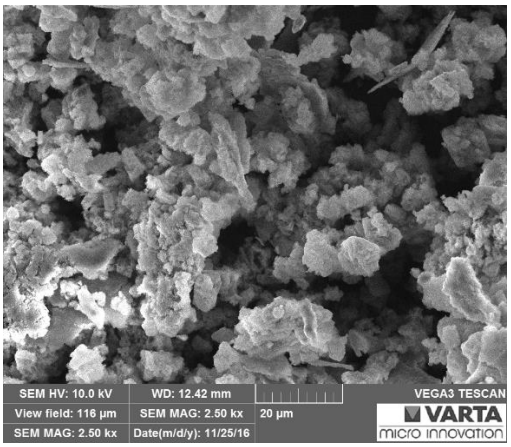

Fig. 25: SEM of the first LiOH lithiation
A change in structure can be seen.

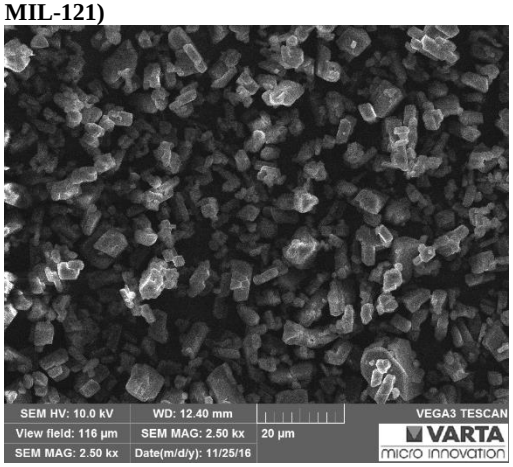

Fig. 26: SEM image after LiAc lithiation
The structure is comparable with the original structure (*Fig. 24*)

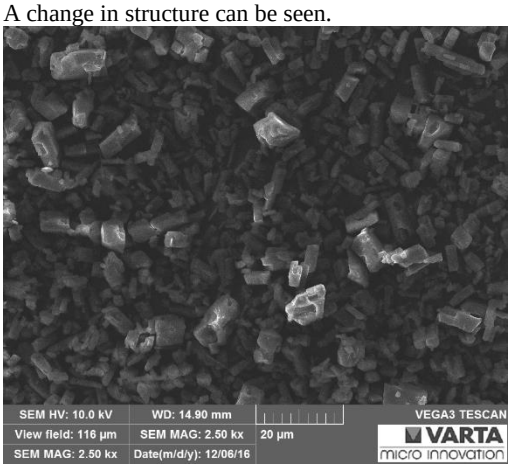

Fig. 27: SEM image after EtOH esterification
The structure is comparable with the original structure (*Fig. 24*)

4.4 Nuclear Magnetic Resonance (NMR) spectroscopy

4.4.1 Liquid ^{1}H NMR

In order to determine if an esterification is possible with the precursor pyromellitic acid, it was esterified with the same three alcohols (MeOH, EtOH and isopropanol) as MIL-121. *Fig. 28* shows the ^{1}H NMR spectrum of the ethanol esterification. The solvent was deuterated chloroform. The signal at 7.3 ppm was related to the chloroform whereas the signal at zero was from tetramethylsilan (TMS), which is added to the solvent, because it refers to a chemical shift of 0 ppm. The signal at 8 ppm referred to the aromatic ring of the acid. The signals occurring at 4.4 ppm (-CH_2) and 1.4 ppm (-CH_3) were from the ethanol group of the ester. Hereby an esterification of pyromellitic acid was confirmed and also the complete esterification of all carboxylic groups can be confirmed as no additional signals occurred due to one or more free carboxylic group. Besides the esterification of the remaining two alcohols were observed and they were successful, too. [35] The other measured spectra are shown in the appendix.

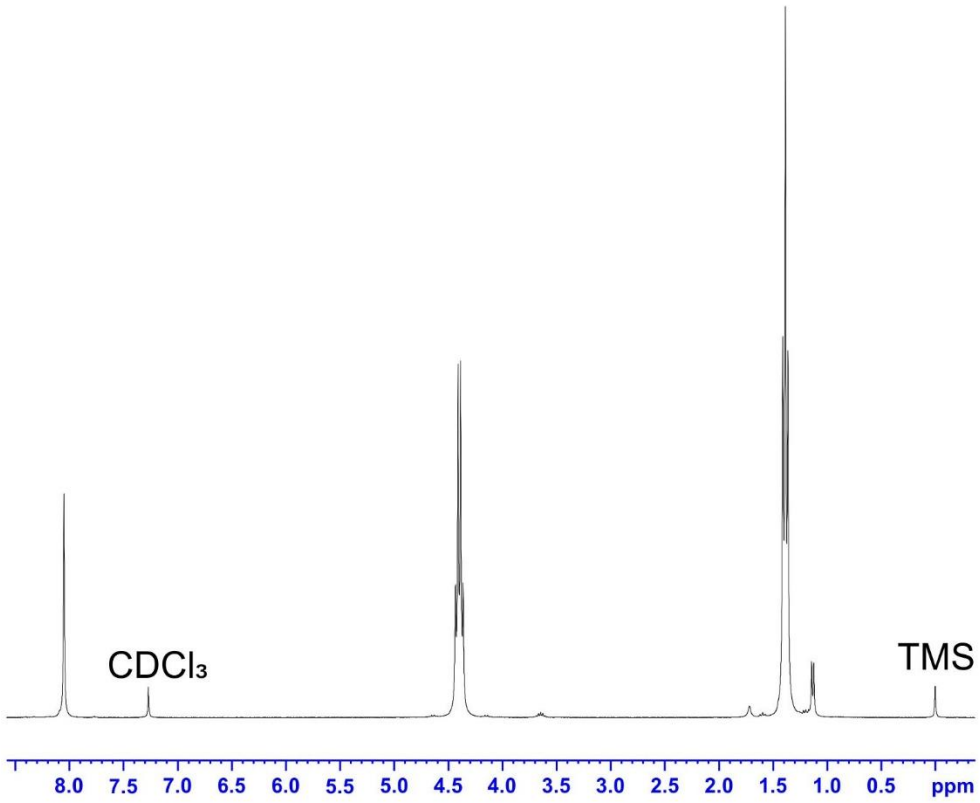

Fig. 28: NMR spectrum of ethanol esterification of pyromellitic acid (solvent: $CDCl_3$)
The signal at 7.3 ppm was related to the chlo-roform whereas the signal at zero was from tetramethylsilan (TMS), which is added to the solvent, because it refers to a chemical shift of 0 ppm. The signal at 8 ppm referred to the aromatic ring of the acid. The signals occurring at 4.4 ppm (-CH2) and 1.4 ppm (-CH3) were from the ethanol group of the ester. Hereby an esterification of pyromellitic acid was confirmed and also the complete esterification of all carboxylic groups can be confirmed as no additional signals occurred due to one or more free carboxylic group.

4.4.2 Solid State NMR

4.4.2.1 ^{7}Li NMR

The observation of sodiated MIL-121 (*4.1 Sodium Hydroxide Titration*) implicates that the lithiation of MIL-121 could in principle work. To confirm Li in the structure, ^{7}Li NMR measurements were carried out with the solid samples. As example *Fig. 29* shows an overlay of ^{7}Li NMR line spectrum of MIL-121 lithiated with LiAc. Li could be detected, which could be seen through the lines occurring at 0 kHz. All other samples measured, except MeOH and isopropanol esterified samples soaked with ionic liquid appeared to contain Li. Samples without Li have to be re-prepared and re-measured to confirm a successful lithiation.

In addition to the confirmation of lithiation, the confirmation of Li motion in the structure can be obtained by ^{7}Li NMR. If motional narrowing occurs than one can conclude that Li ions move in the lattice. Therefore, different temperatures are applied and by increasing the temperature, the lines should narrow, as ions move faster at higher temperatures. This could not be observed at the sample lithiated by LiAc. All measured ^{7}Li NMR spectra where Li was detected are displayed in the appendix. MeOH and isopropanol esterified samples soaked with DMC showed poor signals at 40 and 80 °C and therefore no measurement at lower temperature was carried out.

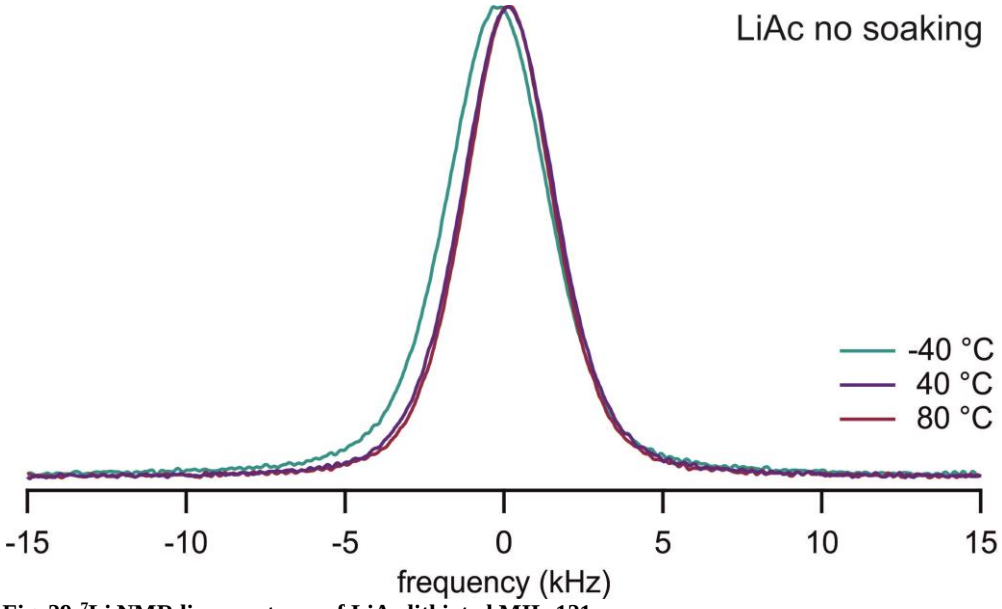

Fig. 29:^{7}Li NMR line spectrum of LiAc lithiated MIL-121
No soaking liquid was added. No motional narrowing could be observed at the sample lithiated by LiAc.

Fig. 30 shows an example of motional narrowing which significantly occurred at just one of the measured samples (*EtOH_DMC30*). All other samples showed only slight narrowing or no narrowing of lines at all.

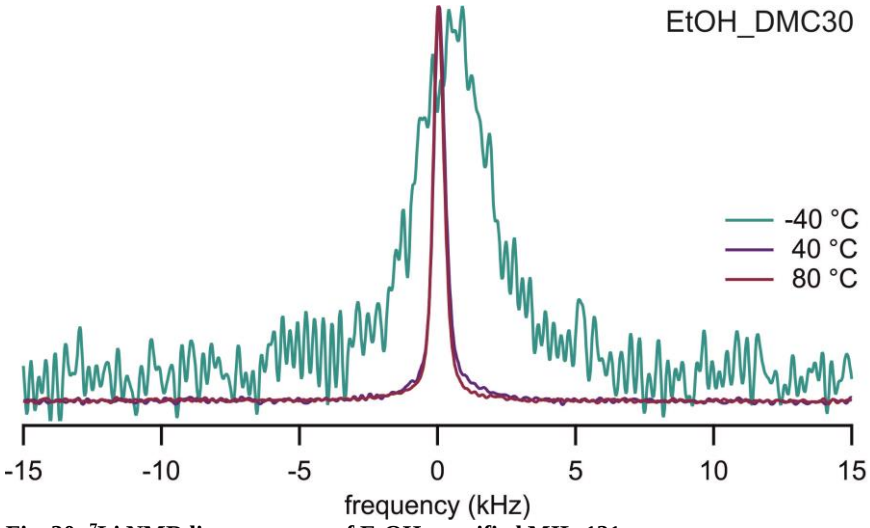

Fig. 30: ^{7}Li NMR line spectrum of EtOH esterified MIL-121
30 wt% of DMC was added as soaking liquid. Motional narrowing occurs from −40 °C to 40 °C but not from 40 °C to 80 °C.

In *Fig. 31* the full width of the NMR-derived lines at half maximum of intensity (fwhm) is plotted against 1000 divided by the absolute temperature. Here it can be seen that also *e.g.* MIL-121 lithiated with LiOH and different soaking liquids (filled squares in different colours) showed little narrowing of the lines. A significant narrowing was observed only at MIL-121 esterified with EtOH and soaked with DMC (open cycles, connected by a light blue line).

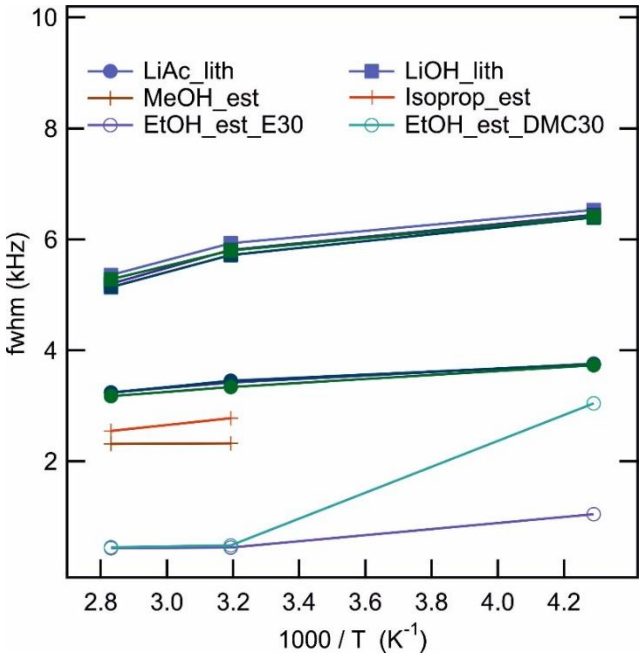

Fig. 31: Fwhm of ^{7}Li NMR lines plotted against 1000 / T
The full width of the NMR-derived lines at half maximum of intensity (fwhm) is plotted against 1000 divided by the absolute temperature T. Here it can be seen that also *e.g.* MIL-121 lithiated with LiOH and different soaking liquids (filled squares in different colours) showed little narrowing of the lines. A significant narrowing was observed only at MIL-121 esterified with EtOH and soaked with DMC (open cycles, connected by a light blue line)

4.4.2.2 ^{1}H MAS NMR

In order to confirm the esterification ^{1}H MAS NMR spectroscopy was carried out. MIL-121 was analysed before and after esterification to observe changes. Furthermore, the precursor pyromellitic acid was esterified and analysed to compare it with MIL-121, which can be found in the appendix.

Fig. 32 shows MIL-121 before esterification. Like in *Fig. 33* (MIL-121 after esterification with EtOH) two dominant signals occurred. The first broad signal consisting of two emerged signals (*Fig. 32*) is different from after isopropanol esterification where at least three signals could be seen. Therefore, a successful esterification was supposed. Moreover, the ^{1}H MAS spectra of two additional esterification attempts (MeOH, isopropanol) are shown in the appendix and lead also to changes from the original structure.

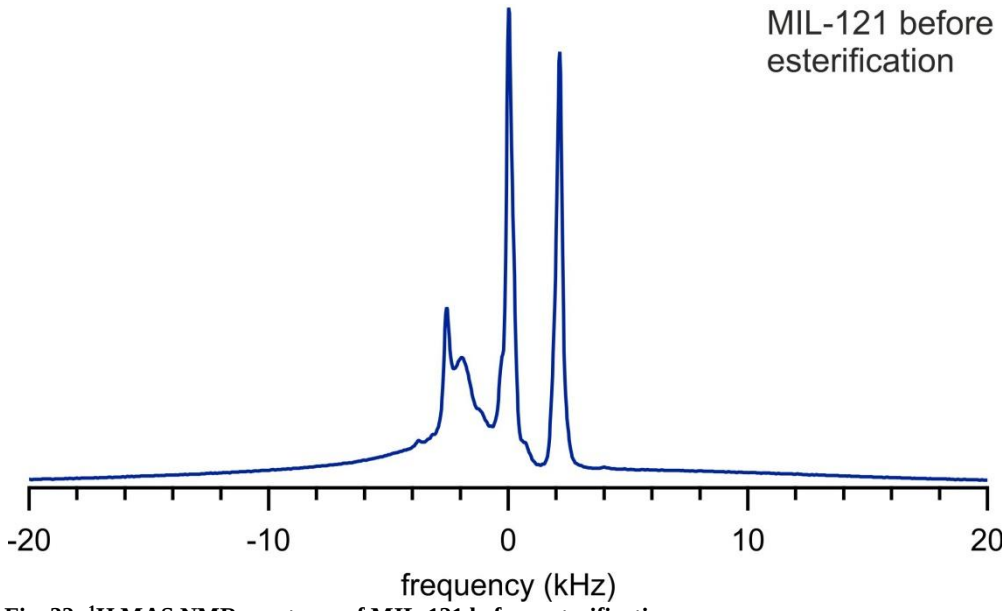

Fig. 32: ^{1}H MAS NMR spectrum of MIL-121 before esterification
Two dominant signals occurred in addition to a broad signal consisting of two emerged signals. The spectrum is used to compare it with the spectrum in after esterification (Fig. 33).

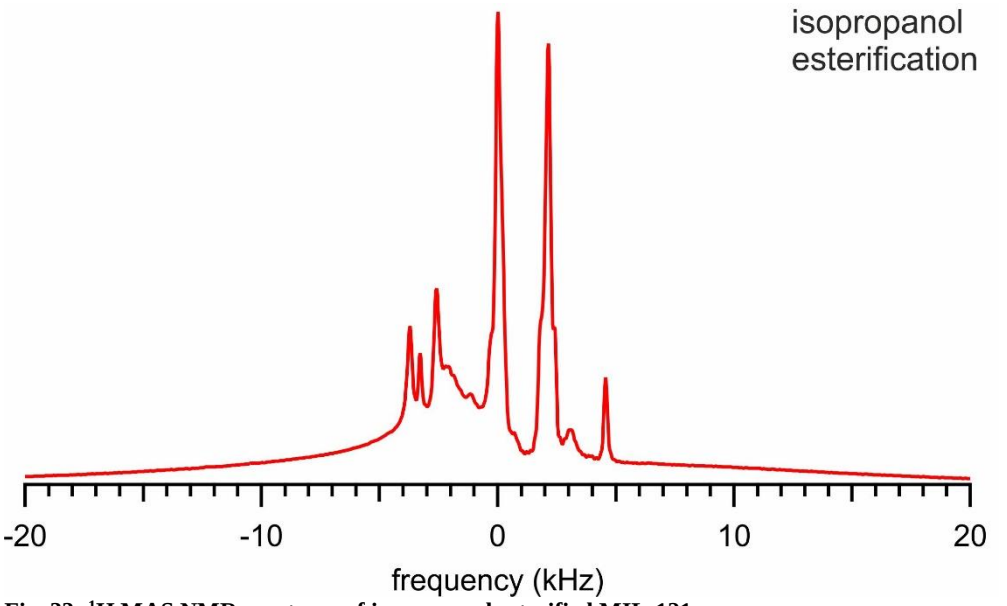

Fig. 33: ^{1}H MAS NMR spectrum of isopropanol esterified MIL-121
Like in Fig. 32 (MIL-121 before esterification with EtOH) two dominant signals occurred. The first broad signal consisting of at least three signals in contrast to the spectrum before esterification. Therefore, a successful esterification was supposed.

However, this is a vague interpretation of the spectra and for an exact confirmation of a successful esterification a broad knowledge of spectra interpretation is necessary. Goldberg *et. al.*[35] and Hesse *et. al.*[36] wrote a publication and a book, respectively which can serve to help understanding these NMR spectra.

4.5 Impedance Spectroscopy (IS)

Samples esterified with MeOH were not measured by IS because the amount of sample was too little. According static ^{7}Li NMR, samples esterified with MeOH and isopropanol and additionally soaked with EMIM-TFSI should not show Li ionic conductivity, because no Li was found in the samples. Nevertheless, the isopropanol esterified sample showed ionic conductivity. This conductivity came from the TFSI ions of the ionic liquid. Although a high intrinsic conductivity of the ionic liquid does not exclude efficient Li transport, a high Li ion conductivity was doubted. Samples without ionic liquids but diglyme, tetraglyme and DMC were measured. These samples showed extremely low ionic conductivity, if it, in fact, can be interpreted as ionic conductivity or rather dielectric losses. Most likely one can see a conductivity plateau at the isopropanol esterification modified MIL-121 soaked with 20 wt% of DMC. (*Fig. 34*) The plateau occurred at low frequencies with a value of $2 \cdot 10^{-12}$ S cm^{-1}. In general, lighter and mobile ions (e.g. Li^{+}) show DC-plateaus extending at lower frequencies, whereas heavier ions (e.g. $TFSI^{-}$) show DC-plateaus only at higher frequencies. It was not clear if there is a plateau at *DMC – 30 wt%* between 10 and 1000 Hz. In principle a higher amount of soaking liquid should lead to higher conductivities as it is seen at the ionic liquid soaked samples. (*Fig. 35* - *Fig. 38*) Most of these samples were better pressable and did not suffer from breaking during sample preparation (e.g. gold coating), because the somewhat viscous ionic liquid worked as a kind of binder. Samples soaked with the second ionic liquid (BMIM-SCN) showed higher ionic conductivity with distinct plateaus (coming from SCN ions) like EMIM-TSFI soaked samples (*Fig. 38*). All graphs are shown in double logarithmic scale.

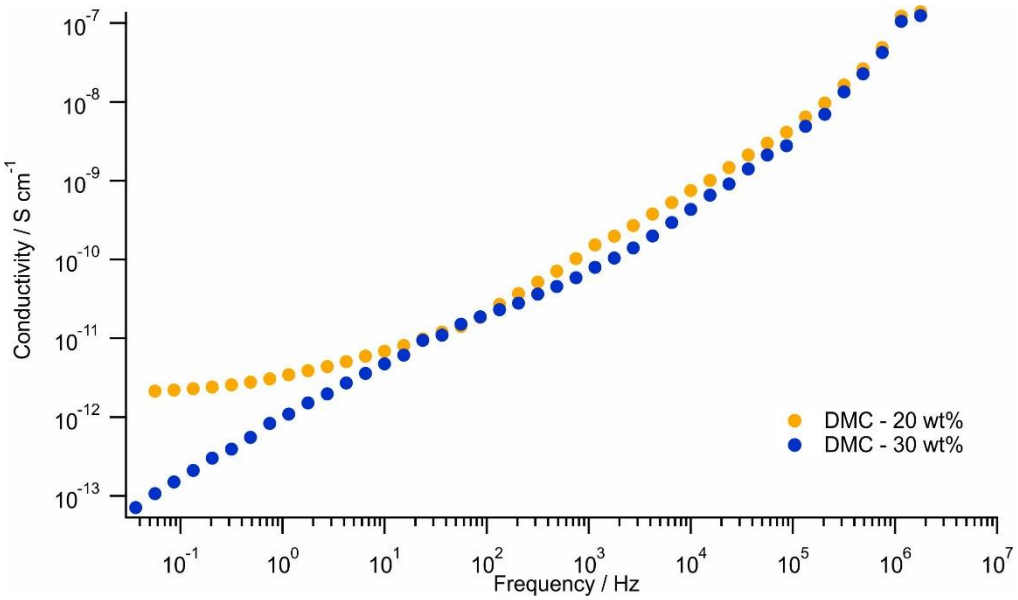

Fig. 34: Conductivity spectra of MIL-121 after isopropanol esterification
The soaking liquid was DMC in different amounts (20 and 30 wt%).
Extremely low ionic conductivity, if it, in fact, can be interpreted as ionic conductivity or rather dielectric losses can be seen in the figure. Most likely there is a conductivity plateau at the isopropanol esterification modified MIL-121 soaked with 20 wt% of DMC (yellow points). The plateau occurred at low frequencies with a value of 2 · 10−12 S cm−1.

Since all the values for conductivity are still low, even if it was Li ion conductivity, those values are not further discussed. The plateaus occurring in the conductivity spectra would be the values for ionic conductivity of the materials. In the following qualitative comparisons of measured samples are discussed.

Fig. 35 shows a measurement series of the LiOH titration samples. Here the soaking liquid was EMIM-TFSI in different amounts (10 – 40 wt%). It can be seen that the higher the amount of soaking liquid the higher the ionic conductivity of the sample. This trend will appear throughout all the measurements.

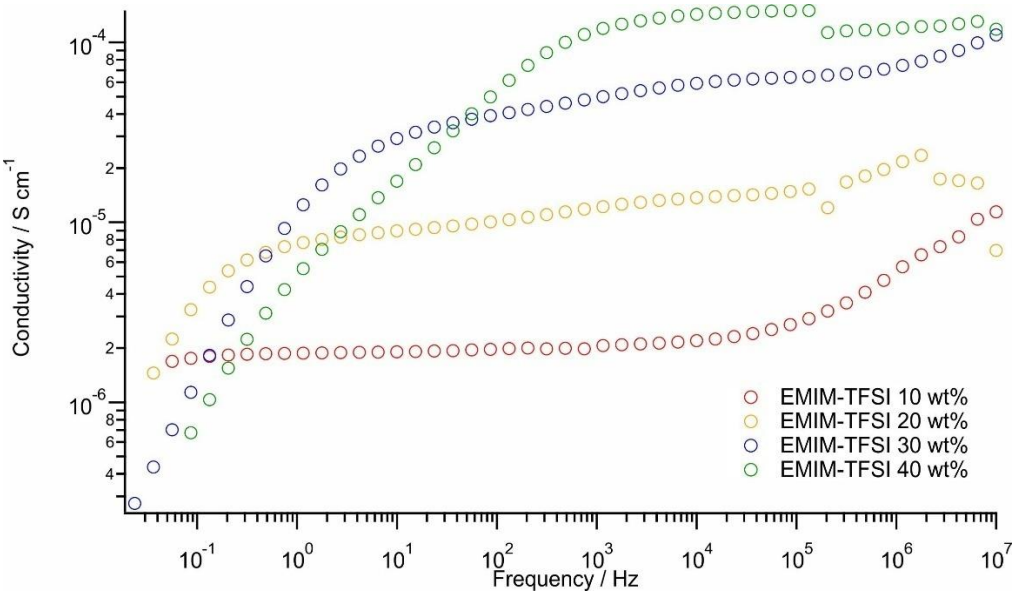

Fig. 35: Conductivity spectra of MIL-121 after LiOH lithiation
The soaking liquid was EMIM-TFSI in different amounts (10, 20, 30 and 40 wt%). It can be seen that the higher the amount of soaking liquid the higher the ionic conductivity of the sample. This trend will appear throughout all the measurements.

Fig. 36 compares the different post synthetic modifications (PSM). Ethanol esterification and LiAc lithiation exceeded isopropanol esterification and LiOH lithiation. The main reason of the different ionic conductivity of the modified MIL-121 samples is the difference in structure. In section *4.2 X-ray Powder Diffraction (XRD)* it was shown that the structure of PSM with LiAc and EtOH were in good agreement with the original structure. Besides, isopropanol esterified and MIL-121 treated with LiOH showed significant deviations from the structure of the starting material. Therefore, maintaining the structure of MIL-121 during PSM is a crucial point for good ionic conductivity.

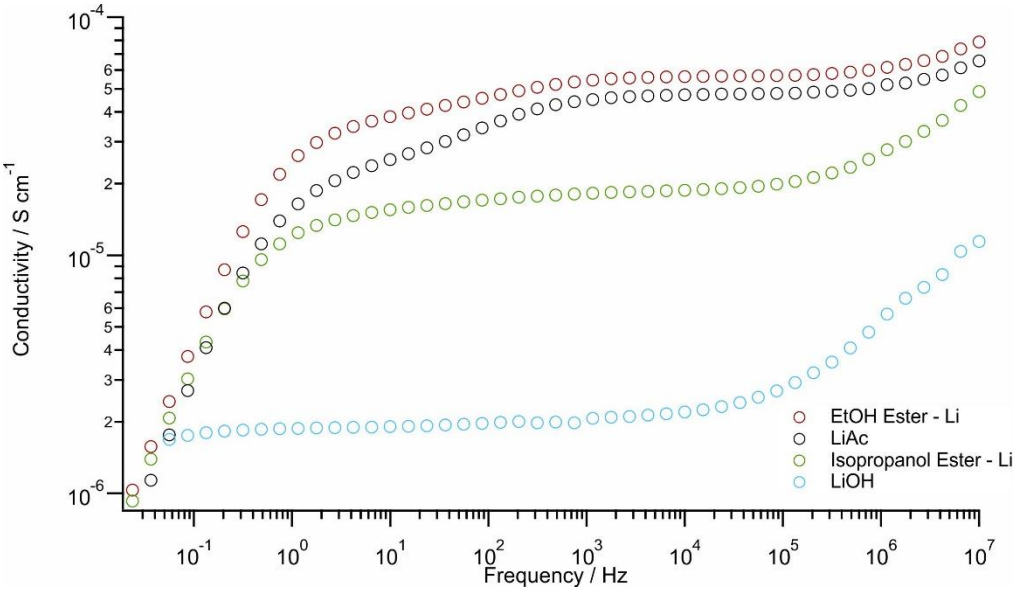

Fig. 36: Conductivity spectra of different PSMs of MIL-121.
The soaking liquid was EMIM-TFSI for LiAc and LiOH and EMIM-TFSI (+LiTFSI; 0.4 M) with a concentration of 10 wt%.
It was shown that the structure of PSM with LiAc and EtOH were in good agreement with the original structure. Besides, isopropanol esterified and MIL-121 treated with LiOH showed significant deviations from the structure of the starting material. Therefore, maintaining the structure of MIL-121 during PSM is a crucial point for good ionic conductivity.

MIL-121 suffers from pores which are filled with residual pyromellitic acid and H_2O from synthesis. Pyromellitic acid was removed by thorough washing and H_2O was removed with vacuum drying at temperatures indicated by TGA. Two of those temperatures (*isoprop_est*: 165 °C, *LiOH_lith*: 220 °C) from TGA were low compared to the others (280 °C). In addition, Volkringer *et. al.* [32] suggests to dry at higher temperature. Due to these facts samples treated with isopropanol and LiOH were dried at 280 °C. *Fig. 37* shows a comparison of *LiOH_lith* samples at two different drying temperatures (HT: 280 °C, LT: 220 °C) and two different soaking concentrations (10 and 30 wt%). It was clearly shown that raising the temperature for drying had adverse effects on the ionic conductivity. Since it is mentioned by Volkringer *et. al.*[32] that higher drying frees the pores, it should be done before PSM. However, PSM has to be changed to water-free substances in order to prevent H_2O-entering of the pores again.

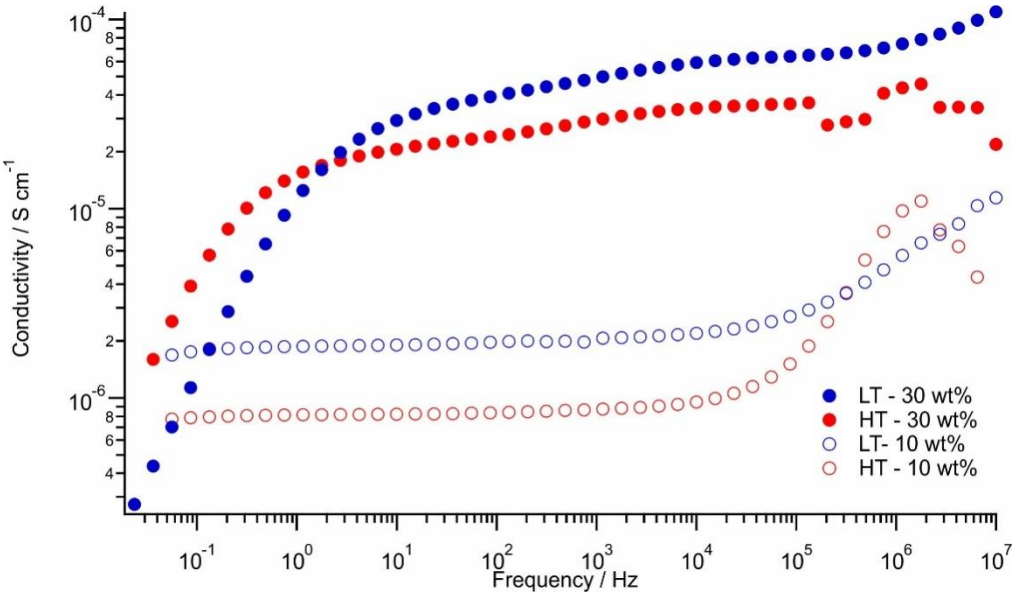

Fig. 37: Conductivity spectra of MIL-121 after LiOH lithiation
The samples were dried at different drying temperatures. The soaking liquid was EMIM-TFSI with a concentration of 10 and 30 wt%, respectively. LT symbolizes low temperature (220 °C) and HT symbolizes high temperature (280 °C). It was clearly shown that raising the temperature for drying had adverse effects on the ionic conductivity.

LiTFSI is poorly soluble in EMIM-TFSI with a maximum concentration of 0.4 M. In order to increase the concentration, ionic liquids with higher LITFSI solubility were found. In BMIM-SCN the concentration of LiTFSI can reach 1.3 M[33] and therefore BMIM-SCN with LiTFSI dissolved was applied to soak the esterified samples. In *Fig. 38* EMIM-TFSI and BMIM-SCN are compared. The expected increase due to higher Li^+ concentration in the samples did not appear. In contrary, BMIM-SCN soaked samples lead to a decrease in conductivity. As mentioned the main part of this shown ionic conductivity is due to the ions of the ionic liquid. Therefore, it can be said that TFSI ions move easier in the lattice than SCN ions do, but an increase or decrease in Li ion conductivity could not be determined.

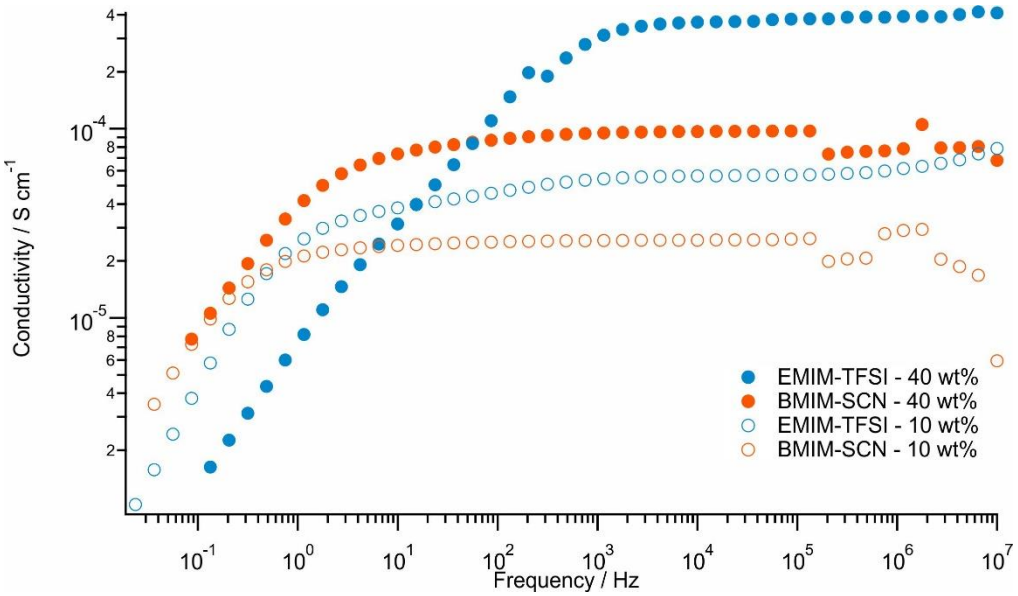

Fig. 38: Conductivity spectra of MIL-121 after ethanol esterification
The soaking liquids were EMIM-TFSI and BMIM-SCN with a concentration of 10 and 40 wt%, respectively. The expected increase due to higher Li+ concentration in the samples did not appear.

Additional conductivity measurements are plotted in the appendix. These graphs show samples with equal PSM but different soaking and drying temperature. Additional measurements of samples without soaking (LiAc and LiOH lithiated samples) and without soaking different from ionic liquid shown in the appendix, too.

4.6 Polarization Experiment

In order to stabilize the cell before the polarization experiment galvanostatic cycling with potential limitation (GCPL) was carried out. Additionally, slight voltage plateaus can be seen which indicated Li^+ insertion and extraction, signifying that, to a certain extend the cell worked. This proved Li ion motion through the built-in electrolyte (LiAc lithiated MIL-121 soaked with EMIM-TFSI 30 wt%), which was not absolutely certain after impedance spectroscopy. *Fig. 39* shows cycles four to six of the GCPL experiment.

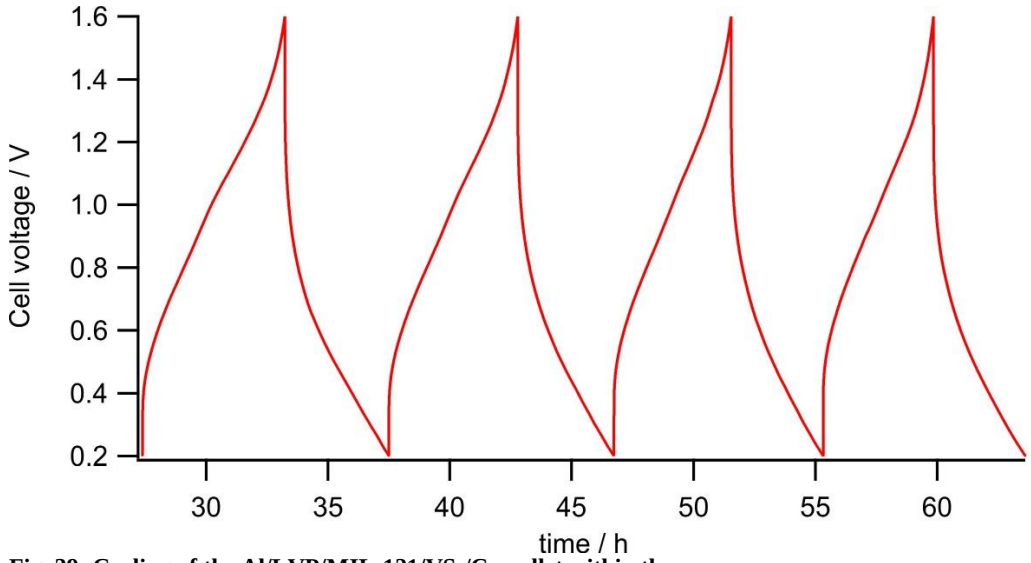

Fig. 39: Cycling of the Al/LVP/MIL-121/VS_2/Cu pellet within the press
Cycles four to six of the GCPL experiment are plotted.

Fig. 40 shows the result of the polarization experiment. It was carried out to calculate the transport number of Li^+ with the Bruce-Vincent-Method (BVM). The ratio between equilibrium and starting current results in the transport number. In this case the current passes the abscise at zero and therefore BVM could not be applied. The reason for this was most likely the fact that the cell was not symmetric or that self-discharge of the cell occurs during the experiment. Normally the electrodes are out of the same material when BVM is applied. Moreover, the method is typically used for polymer electrolytes. A requirement for applying the Bruce-Vincent-Method is a known impedance which is measured before and after the polarization experiment. (*Fig. 41*)

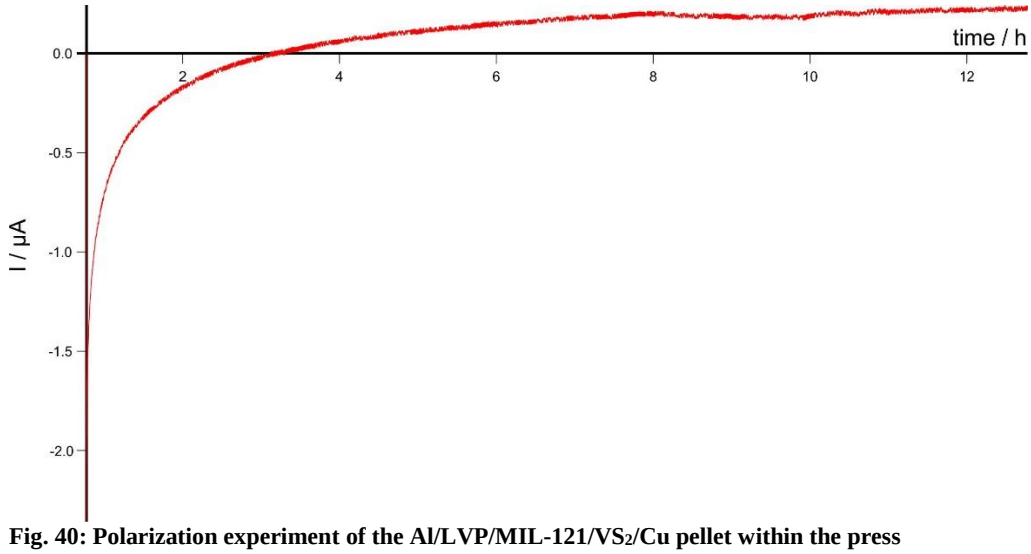

Fig. 40: Polarization experiment of the Al/LVP/MIL-121/VS_2/Cu pellet within the press

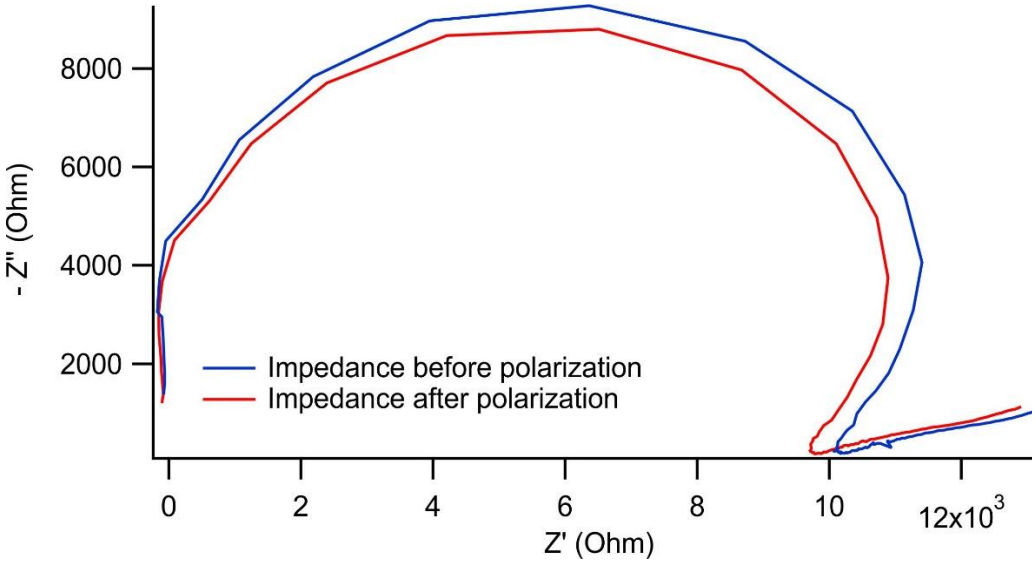

Fig. 41: Nyquist plot of the Al/LVP/MIL-121/VS_2/Cu pellet within the press before (blue) and after (red) the polarization experiment

5 Conclusion

Preliminary examination of PSM with ^{1}H MAS NMR spectroscopy to confirm esterification and ^{7}Li NMR spectroscopy to confirm lithiation lead to a confirmation that the reactions were successful. Confirmation of esterification of the precursor pyromellitic acid resulted in a positive result and a complete esterification of all four carboxylic groups with the corresponding alcohols (MeOH, EtOH, isopropanol) could be observed.

SEM images and XRD of the samples showed that a lithiation approach with excess LiOH had to be modified. The high pH value destroyed the structure of MIL-121. A titration technique where LiOH was added in lower concentration and in steps was successful and the structure could be maintained. The XRD measurements showed that LiAc lithiated and EtOH esterified samples showed best retention of structure in comparison to the starting material whereas a deviation in structure was clearly observable for the different modified samples.

The conductivity measurements showed a trend that, the better the match to the structure of MIL-121 unmodified the better the conductivity of the modified samples. Nevertheless, only samples soaked with an ionic liquid showed conductivities in the order of $\mathbf{10^{-4}}$ **-** $\mathbf{10^{-6}\ S\ cm^{-1}}$. Small Li ion conductivity was found in one sample (isopropanol esterification modified MIL-121 soaked with 20 wt% of dimethyl carbonate) at very low frequencies (0.06 – 1 Hz) where a conductivity plateau was detectable at $\mathbf{2 \cdot 10^{-12}\ S\ cm^{-1}}$.

A final experiment where a cell with MIL-121 (after PSM and soaking) as solid state electrolyte was cycled showed that Li ions can be transported through the lattice. The following polarization experiment did not work, because the electrode were out of different materials. For the Bruce-Vincent-Method to determine the transport number of ions the cell has to be symmetric. Nevertheless, these materials present interesting ion conduction properties that will constitute the object of further investigations.

A. Literature

1. Goodenough, J. B. & Park, K. The Li-Ion Rechargeable Battery : A Perspective. *J. Am. Chem. Soc.* **135,** 1167–1176 (2013).

2. Tarascon, J. M. & Armand, M. Issues and challenges facing rechargeable lithium batteries. *Nature* **414,** 359–67 (2001).

3. Steiger, J. Mechanisms of Dendrite Growth in Lithium Metal Batteries. (2015).

4. Aurbach, D. *et al.* Design of electrolyte solutions for Li and Li-ion batteries: A review. *Electrochim. Acta* **50,** 247–254 (2004).

5. Li, H., Wang, Z., Chen, L. & Huang, X. Research on advanced materials for Li-ion batteries. *Adv. Mater.* **21,** 4593–4607 (2009).

6. Rui, X., Yan, Q., Skyllas-kazacos, M. & Mariana, T. Li 3 V 2 (PO 4) 3 cathode materials for lithium-ion batteries : A review. *J. Power Sources* **258,** 19–38 (2014).

7. Tao, D. *et al.* Lithium vanadium phosphate as cathode material for lithium ion batteries. *Ionics (Kiel).* **21,** 1201–1239 (2015).

8. Dunn, B., Kamath, H. & Tarascon, J.-M. Electrical Energy Storage for the Grid: A Battery of Choices. *Science (80-.).* **334,** 928–935 (2011).

9. Li, J., Ma, C., Chi, M., Liang, C. & Dudney, N. J. Solid electrolyte: The key for high-voltage lithium batteries. *Adv. Energy Mater.* **5,** 1–6 (2015).

10. Knauth, P. Inorganic solid Li ion conductors: An overview. *Solid State Ionics* **180,** 911–916 (2009).

11. Sun, C., Liu, J., Gong, Y., Wilkinson, D. P. & Zhang, J. Recent advances in all-solid-state rechargeable lithium batteries. *Nano Energy* **33,** 363–386 (2017).

12. Bates, J. B. *et al.* Fabrication and characterization of amorphous lithium electrolyte thin films and rechargeable thin-film batteries. *J. Power Sources* **43,** 103–110 (1993).

13. Minami, T. & Tatsumisago, M. No Title. *Solid State Ionics Batter. Springer-Verlag* P1 (2005).

14. Minami, T., Hayashi, A. & Tatsumisago, M. Recent progress of glass and glass-ceramics as solid electrolytes for lithium secondary batteries. *Solid State Ionics* **177,** 2715–2720 (2006).

15. Chowdari, B. V. R., Subba Rao, G. V. & Lee, G. Y. H. XPS and ionic conductivity studies on Li2O-Al2O3-(TiO2 or GeO2)-P2O5 glass-ceramics. *Solid State Ionics* **136–137,** 1067–1075 (2000).

16. Bohnke, O., Bohnke, C. & Fourquet, J. L. J. Mechanism of ionic conduction and electrochemical intercalation of lithium into the perovskite lanthanum lithium titanate. *Solid State Ionics* **91,** 21–31 (1996).

17. Thangadurai, V. & Weppner, W. Li6ALa2Ta2O12 (A=Sr, Ba): Novel garnet-like oxides for fast lithium ion conduction. *Adv. Funct. Mater.* **15,** 107–112 (2005).

18. Li, J., Lin, Y., Yao, H., Yuan, C. & Liu, J. Tuning thin-film electrolyte for lithium battery by grafting cyclic carbonate and combed poly(ethylene oxide) on polysiloxane. *ChemSusChem* **7,** 1901–1908 (2014).

19. Editors, G. *et al.* Metal–organic framework materials as catalysts. *Chem. Soc. Rev.* **38,**

1450–1459 (2009).

20. Bétard, A. & Fischer, R. A. Metal-organic framework thin films: From fundamentals to applications. *Chem. Rev.* **112,** 1055–1083 (2012).

21. Bureekaew, S. *et al.* One-dimensional imidazole aggregate in aluminium porous coordination polymers with high proton conductivity. *Nat. Mater.* **8,** 831–836 (2009).

22. Takaishi, S. *et al.* Electroconductive porous coordination polymer Cu[Cu(pdt)2] composed of donor and acceptor building units. *Inorg. Chem.* **48,** 9048–9050 (2009).

23. Zhu, K., Liu, Y. & Liu, J. A fast charging/discharging all-solid-state lithium ion battery based on PEO-MIL-53(Al)-LiTFSI thin film electrolyte. *Rsc Adv.* **4,** 42278–42284 (2014).

24. Ameloot, R. *et al.* Ionic conductivity in the metal-organic framework UiO-66 by dehydration and insertion of lithium tert-butoxide. *Chem. - A Eur. J.* **19,** 5533–5536 (2013).

25. Wiers, B. M., Foo, M. L., Balsara, N. P. & Long, J. R. A solid lithium electrolyte via addition of lithium isopropoxide to a metal-organic framework with open metal sites. *J. Am. Chem. Soc.* **133,** 14522–14525 (2011).

26. 1,2,4,5-Benzenetetracarboxylic acid. Available at: http://www.sigmaaldrich.com. (Accessed: 13th April 2017)

27. Krischner, H. & Koppelhuber-Bitschnau, B. *Röntgenstrukturanalyse und Rietveldmethode*. (Vieweg, 1994).

28. An Introduction to Single-Crystal X-Ray Crystallography. Available at: http://archive.cnx.org/contents/a1d2bdad-bed2-4b40-aaa2-43e15b3010e4@2/an-introduction-to-single-crystal-x-ray-crystallography#eip-740. (Accessed: 7th April 2017)

29. Stanje, B. Lithium diffusivity in restricted dimensions: diffusion along the inner surfaces and in disordered, nanostructured ionic conductors. (2017).

30. Barsoukov, E. & Macdonald, J. R. *Impedance Spectroscopy: Theory, Experiment, and Applications*. (Wiley, 2005).

31. Lvovich, V. F. *Impedance Spectroscopy - Application to Electrochemical and Dielectric Phenomena*. (Wiley, 2012).

32. Volkringer, C. *et al.* High-throughput aided synthesis of the porous metal-organic framework-type aluminum pyromellitate, MIL-121, with extra carboxylic acid functionalization. *Inorg. Chem.* **49,** 9852–9862 (2010).

33. Rosol, Z. P., German, N. J. & Gross, S. M. Solubility, ionic conductivity and viscosity of lithium salts in room temperature ionic liquids. *Green Chem.* **11,** 1453–1457 (2009).

34. Forsyth, M. *et al.* Novel Na+ Ion Diffusion Mechanism in Mixed Organic-Inorganic Ionic Liquid Electrolyte Leading to High Na+ Transference Number and Stable, High Rate Electrochemical Cycling of Sodium Cells. *J. Phys. Chem. C* **120,** 4276–4286 (2016).

35. Fulmer, G. R. *et al.* NMR chemical shifts of trace impurities: Common laboratory solvents, organics, and gases in deuterated solvents relevant to the organometallic chemist. *Organometallics* **29,** 2176–2179 (2010).

36. Hesse, M., Meier, H. & Bernd, Z. *Spektroskopische Methoden in der organischen Chemie*. (Thieme, 2012).

B. Abbreviations

Ar	argon
B10	soaking with 10 wt% BMIM-SCN (also with 20, 30 and 40 wt%)
BMIM-SCN	1-butyl-3-methylimidazolium thiocyanate
BVM	Bruce-Vincent-Method
diglyme, DG	diethylene glycol dimethyl ether
DMC	dimethyl carbonate
E10	soaking with 10 wt% EMIM-TFSI (also with 20, 30 and 40 wt%)
EDX	energy-dispersive X-ray Spectroscopy
EMIM-TFSI	1-ethyl-3-methylimidazolium bis(trifluoromethylsulfonyl)imide
EtOH	ethanol
est	esterification
GCPL	galvanostatic cycling with potential limitation
IS	impedance spectroscopy
isoprop	isopropanol
KF	Karl Fischer (titration)
Li	lithium
LiAc	lithium acetate
LIB	lithium ion battery
LiOH	lithium hydroxide
LiTFSI	bis(trifluoromethane)sulfonimide lithium salt
lith	lithiation
LVP	lithium vanadium phosphate
MAS	magic angle spinning
MeOH	methanol
Mg	magnesium
MIL	Matériaux de l′Institut Lavoisier
Na	sodium
NMR	nuclear magnetic resonance
PSM	post synthetic modification
RT	room temperature
SHE	standard hydrogen electrode
tetraglyme, TG	tetraethylene glycol dimethyl ether
TGA	thermogravimetric analysis
UiO	Universitetet i Oslo
wt%	weight percentage
XRD	X-ray powder diffraction
Zr	zirconium

C. Appendix

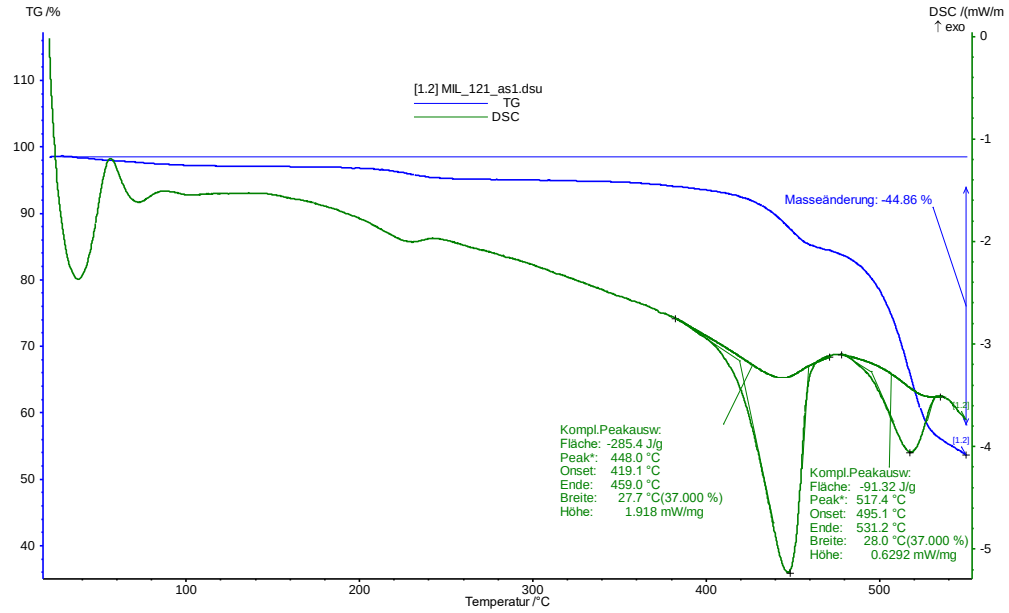

Fig. 42: TGA of MIL-121

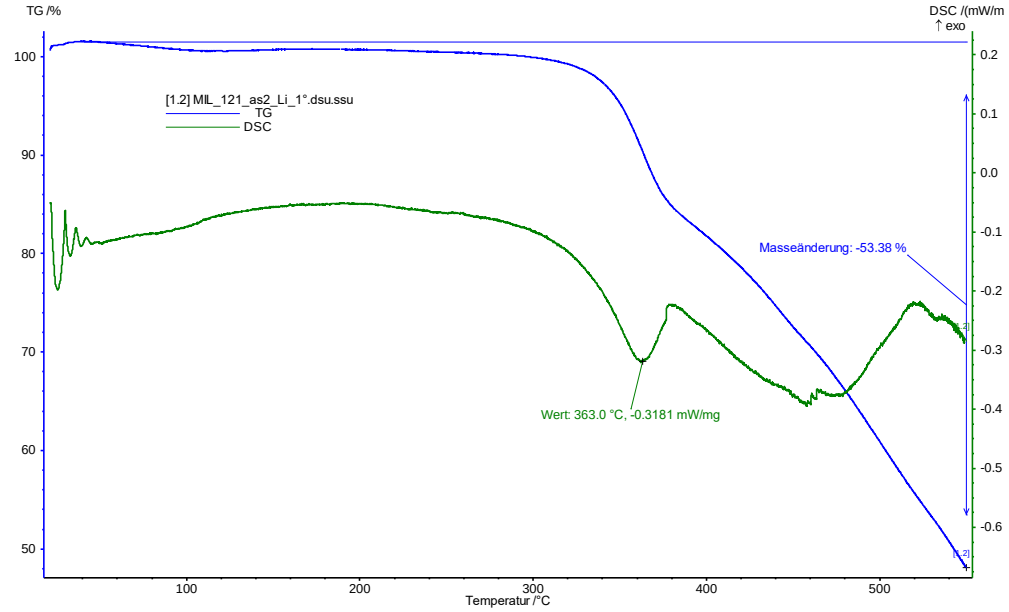

Fig. 43: TGA of LiAc lithiated MIL-121

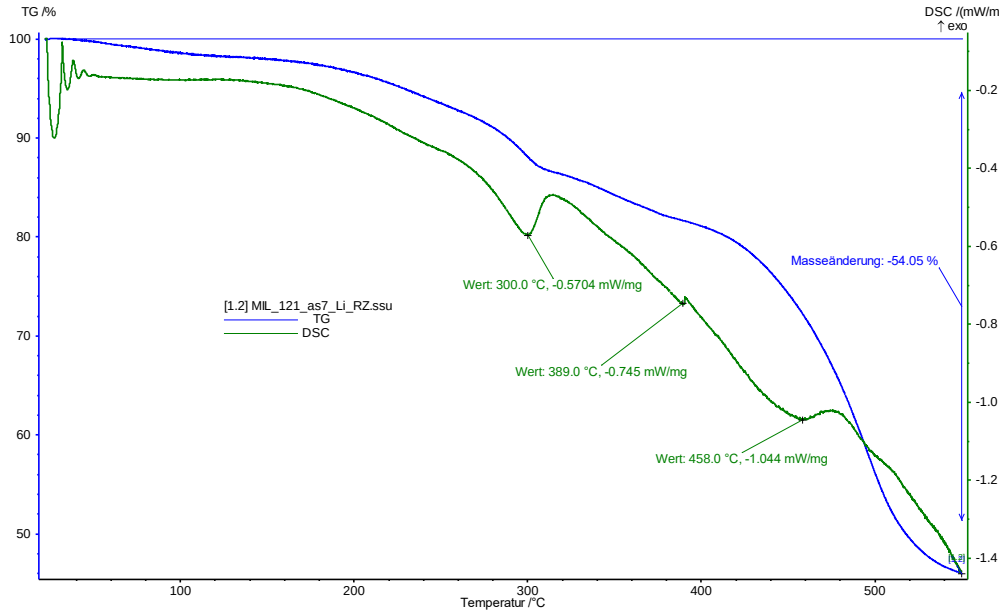

Fig. 44: TGA of LiOH (titration) lithiated MIL-121

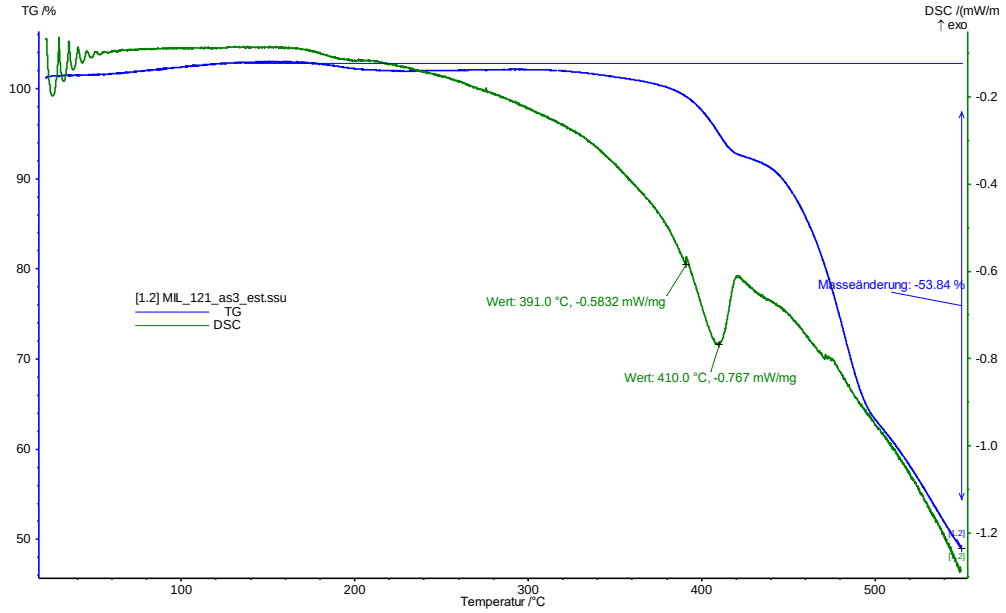

Fig. 45: TGA of EtOH esterified MIL-121

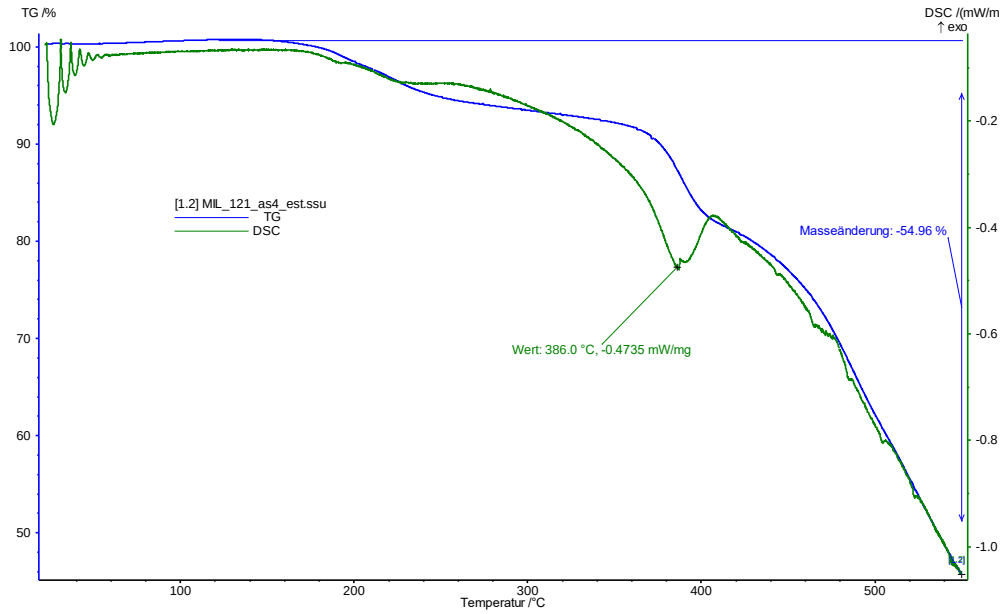

Fig. 46: TGA of MeOH esterified MIL-121

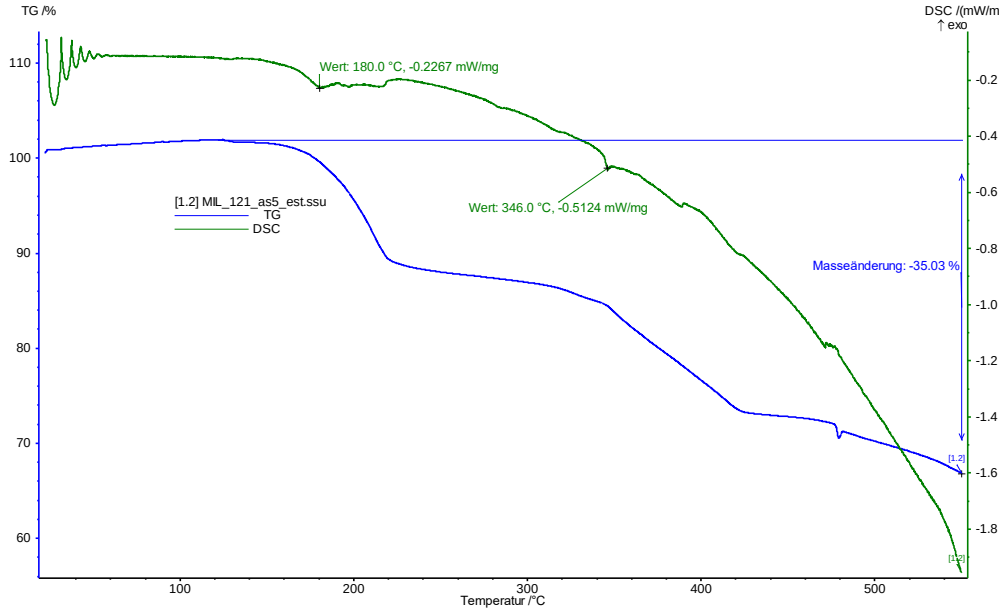

Fig. 47: TGA of Isopropanol esterified MIL-121

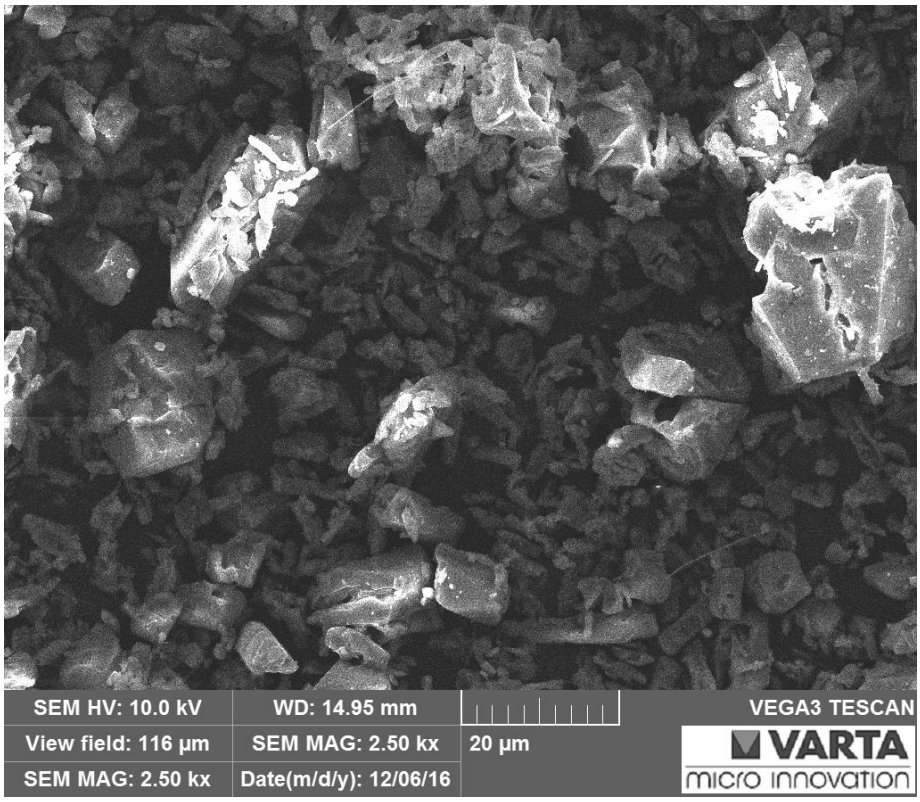

Fig. 48: SEM image after MeOH esterification

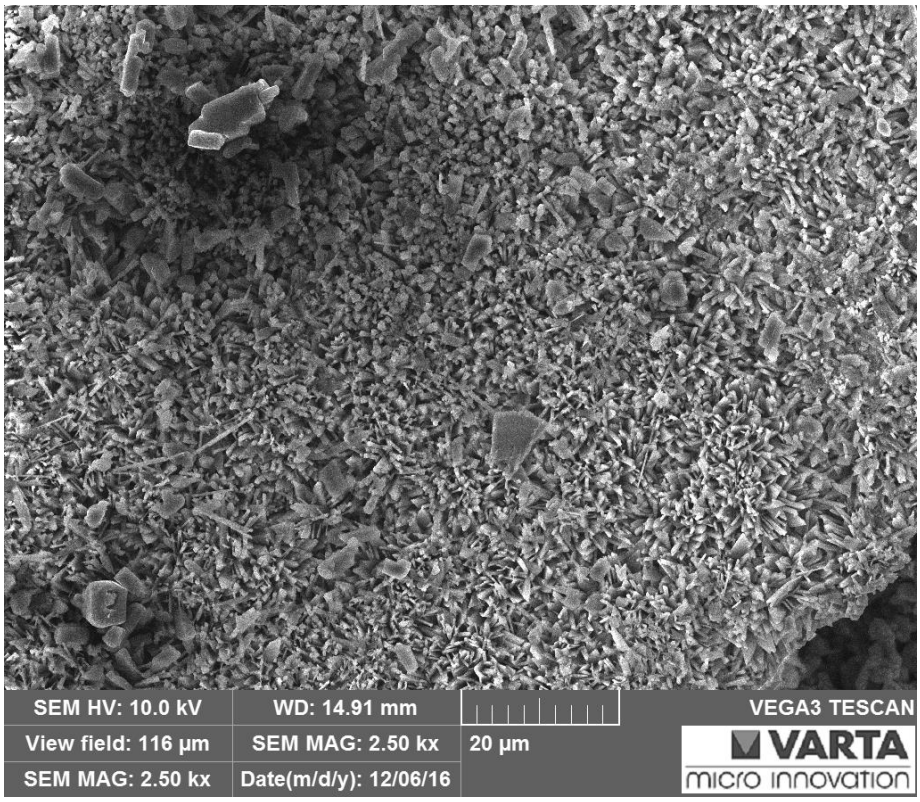

Fig. 49: SEM image after isopropanol esterification

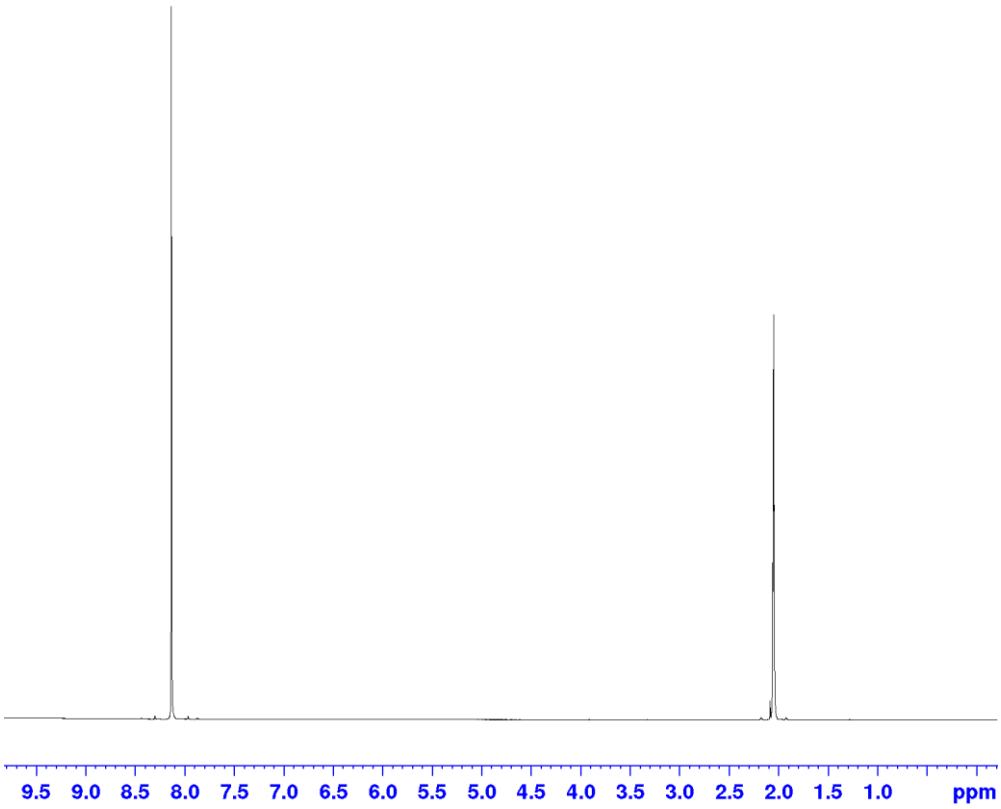

Fig. 50: ^{1}H liquid NMR spectrum of pyromellitic acid (solvent: acetone-d_6)

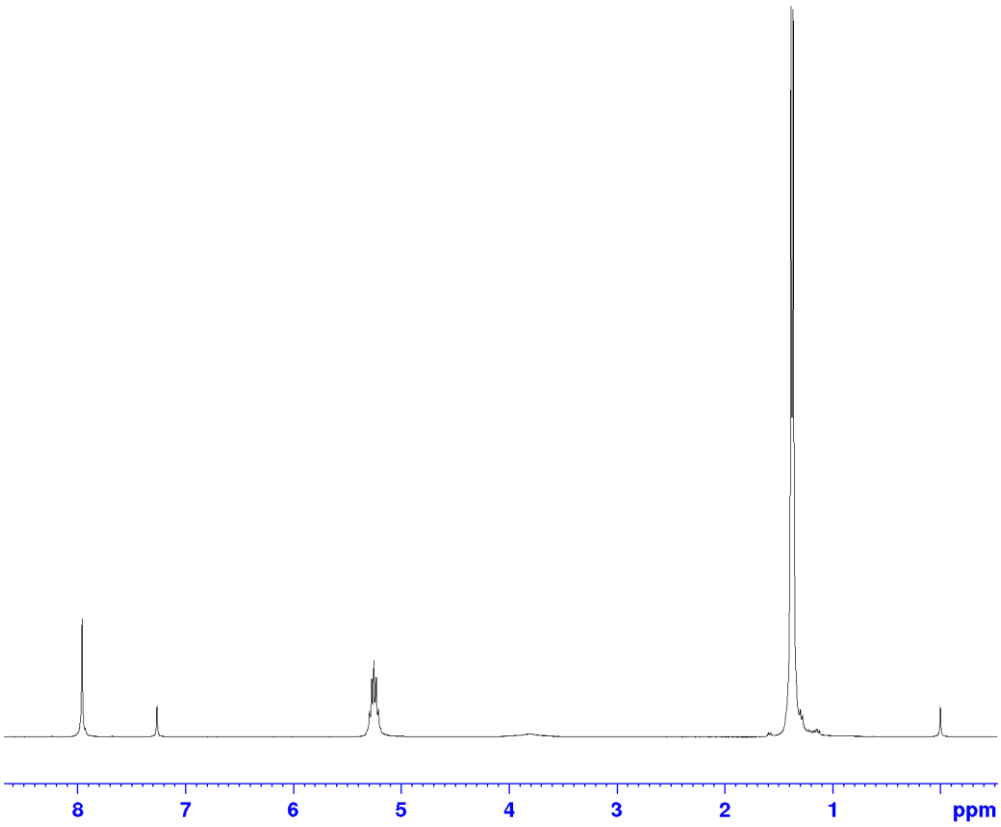

Fig. 51: ^{1}H liquid NMR spectrum of isopropanol esterification of pyromellitic acid (solvent: $CDCl_3$)

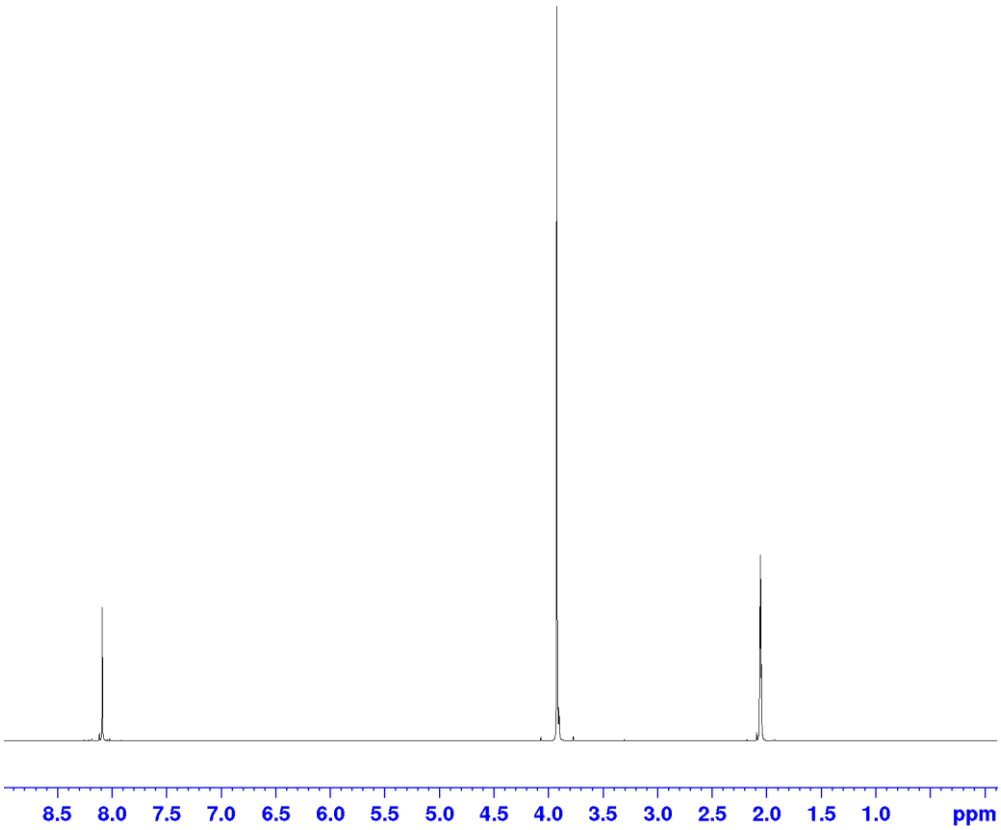

Fig. 52: ^{1}H liquid NMR spectrum of MeOH esterification of pyromellitic acid (solvent: acetone-d_6)

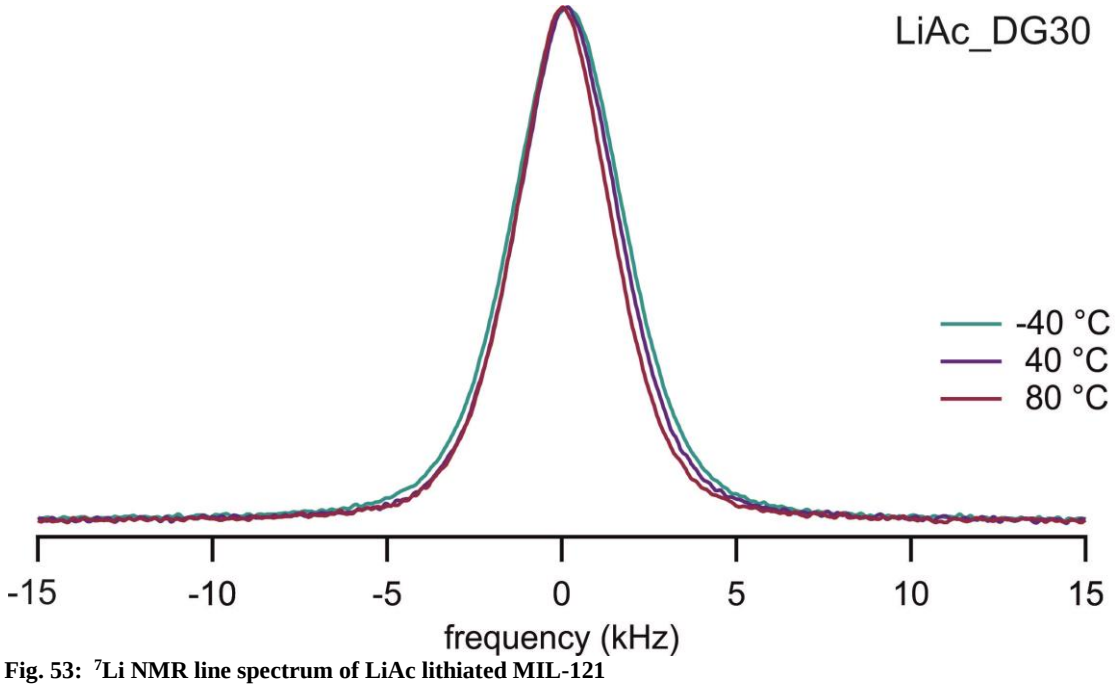

Fig. 53: ^{7}Li NMR line spectrum of LiAc lithiated MIL-121
30 wt% of diglyme was added as soaking liquid.

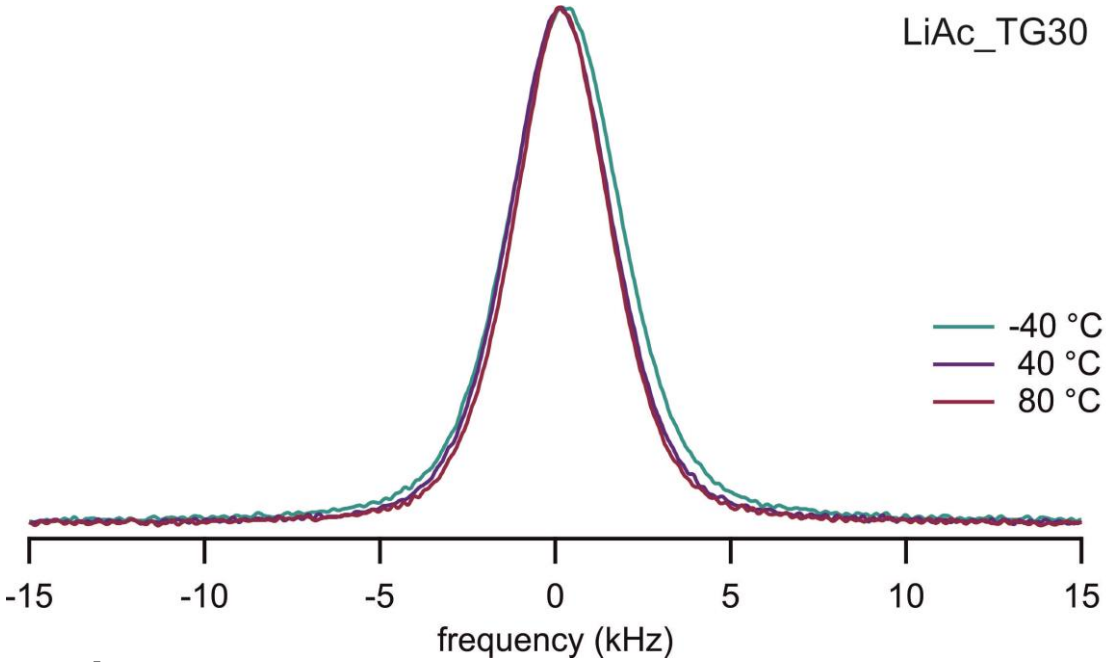

Fig. 54: ^{7}Li NMR line spectrum of LiAc lithiated MIL-121
30 wt% of tetraglyme was added as soaking liquid.

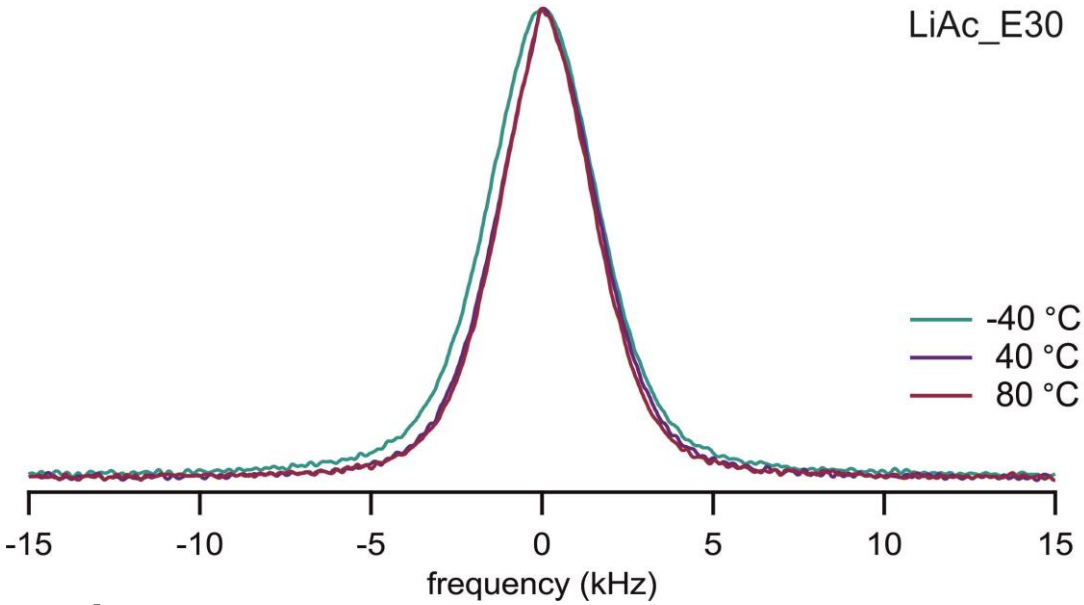

Fig. 55: ^{7}Li NMR line spectrum of LiAc lithiated MIL-121
30 wt% of EMIM-TFSI was added as soaking liquid.

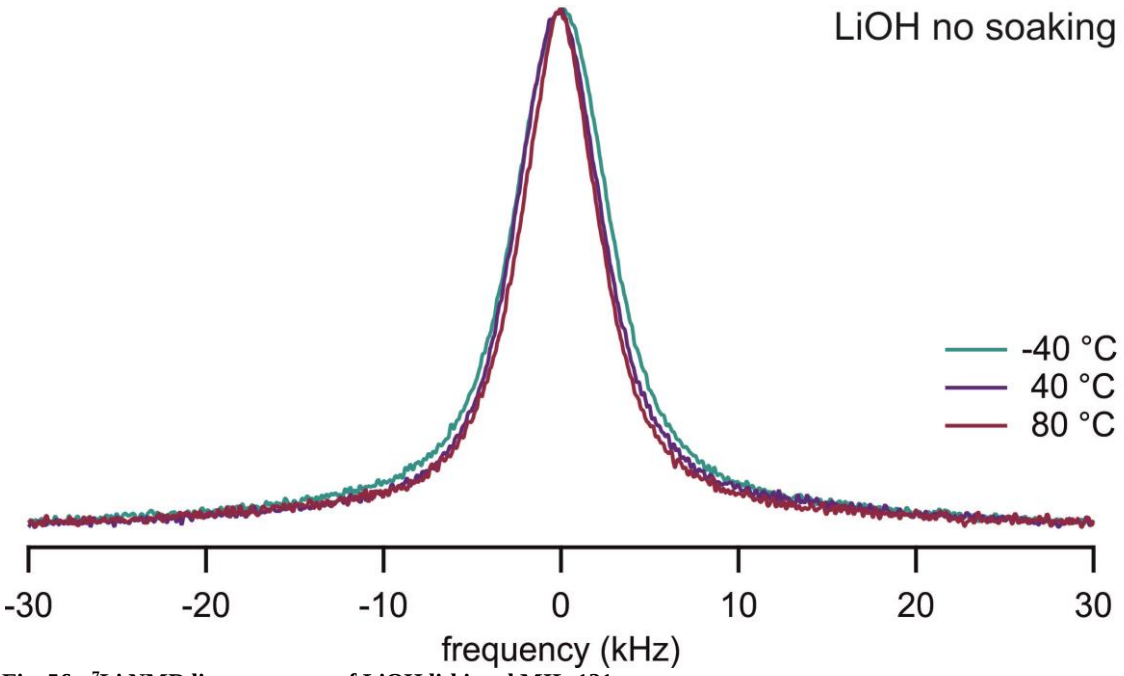

Fig. 56: ^{7}Li NMR line spectrum of LiOH lithiated MIL-121
No soaking liquid was added.

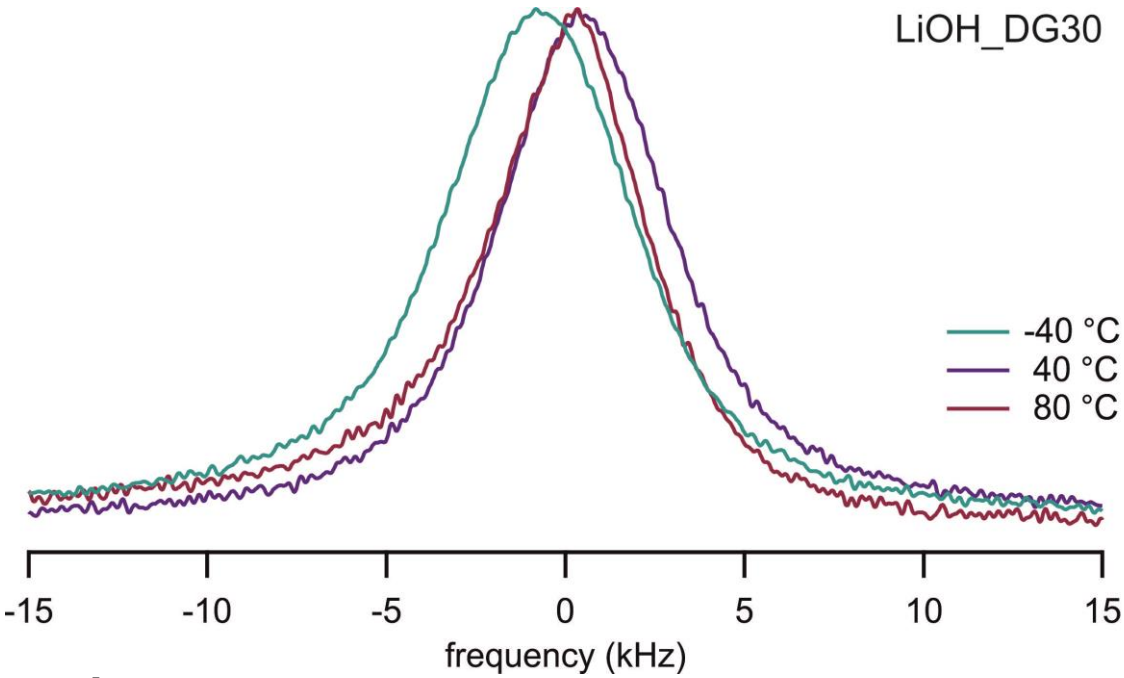

Fig. 57: ^{7}Li NMR line spectrum of LiOH lithiated MIL-121
30 wt% of diglyme was added as soaking liquid.

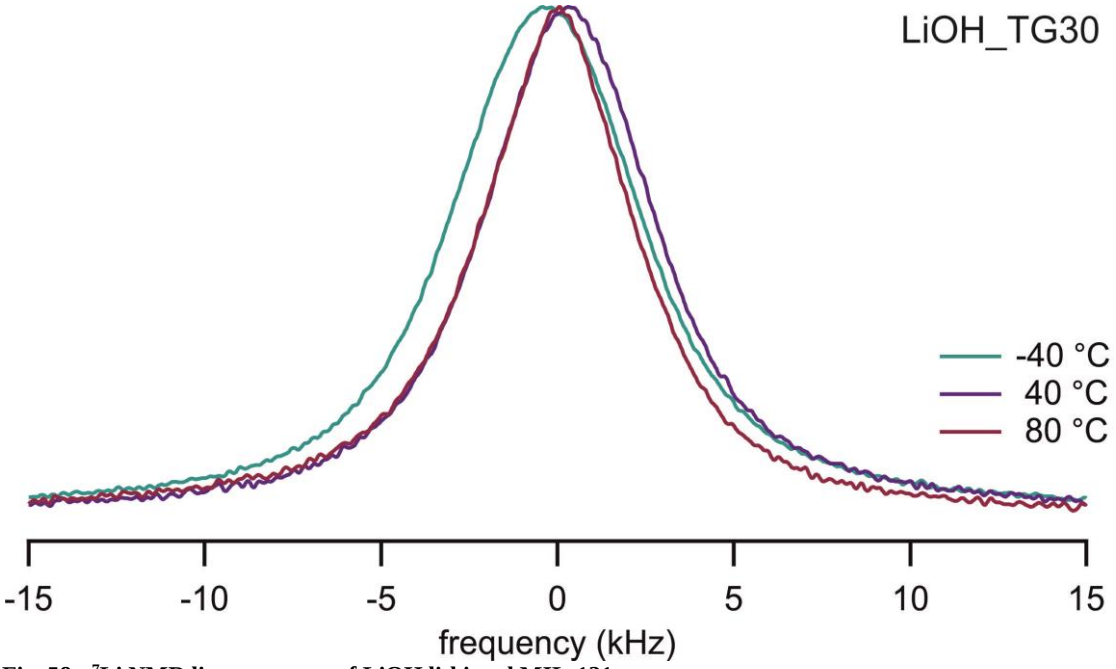

Fig. 58: ^{7}Li NMR line spectrum of LiOH lithiated MIL-121
30 wt% of tetraglyme was added as soaking liquid.

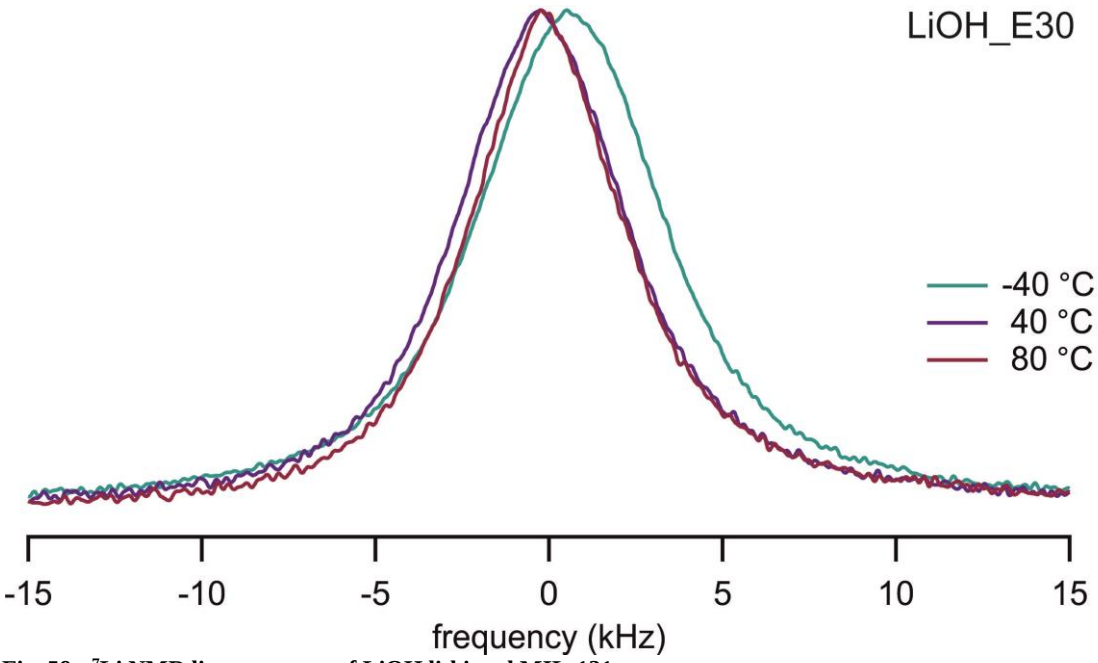

Fig. 59: ^{7}Li NMR line spectrum of LiOH lithiated MIL-121
30 wt% of EMIM-TFSI was added as soaking liquid.

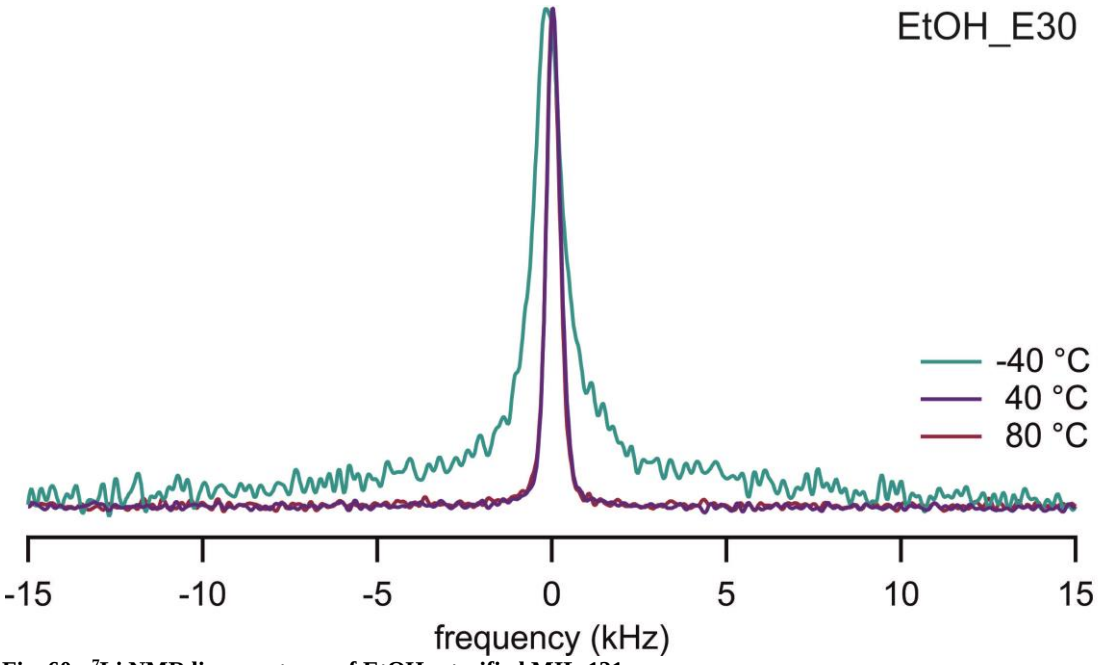

Fig. 60: ^{7}Li NMR line spectrum of EtOH esterified MIL-121
30 wt% of EMIM-TFSI were added as soaking liquid.

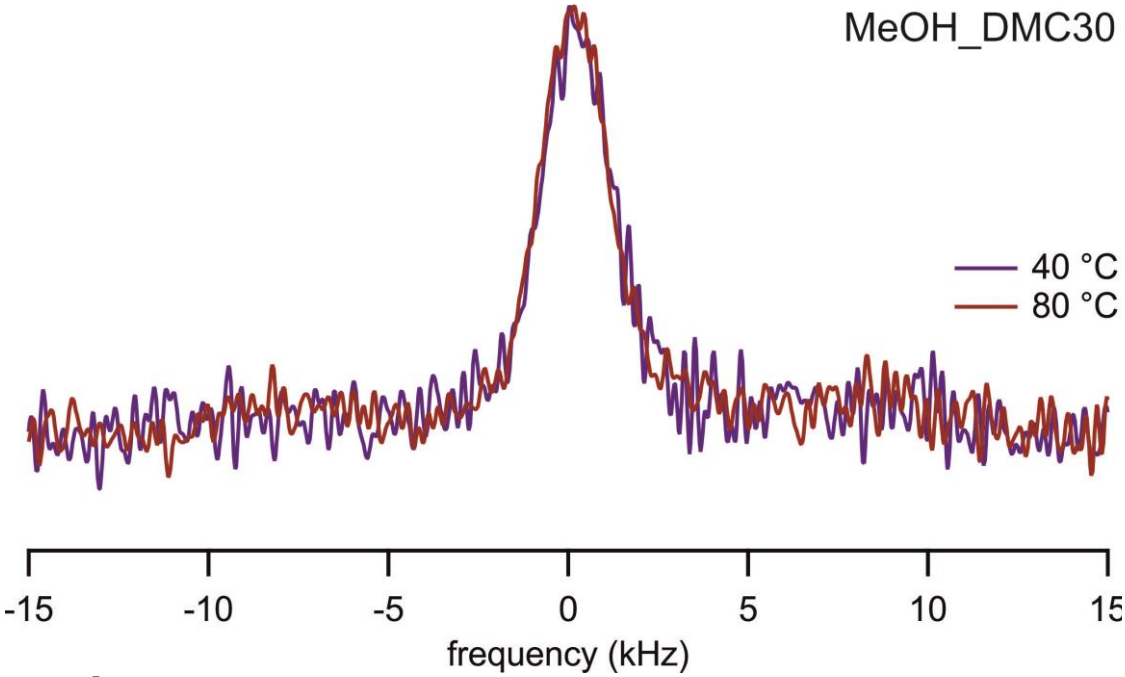

Fig. 61: ^{7}Li NMR line spectrum of MeOH esterified MIL-121
30 wt% of DMC were added as soaking liquid.

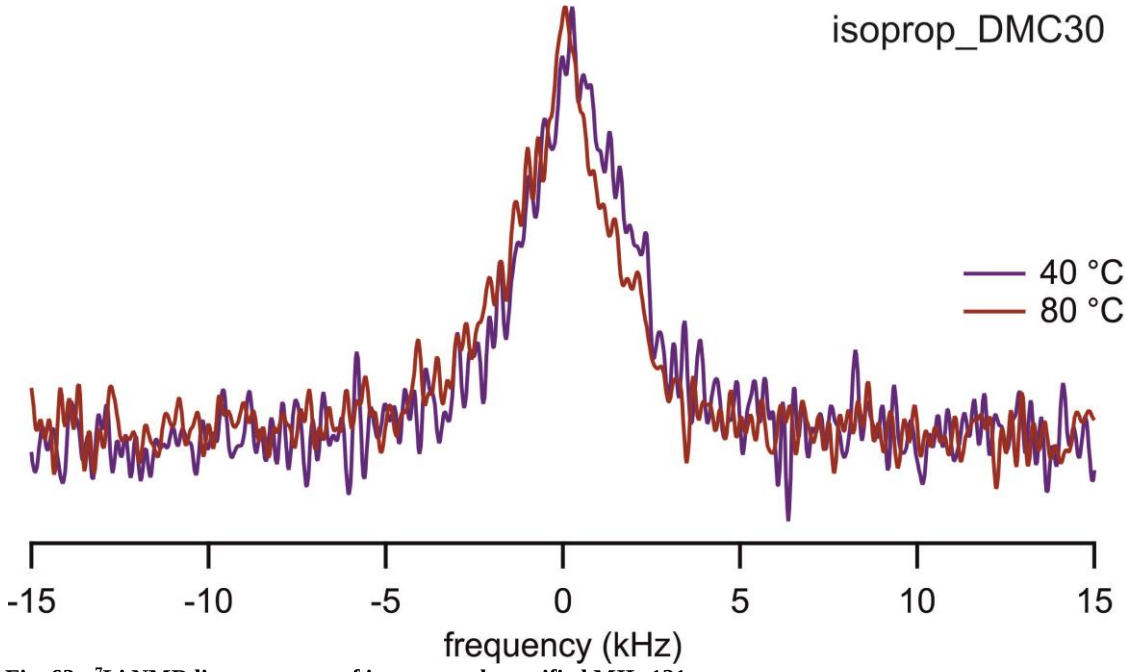

Fig. 62: ^{7}Li NMR line spectrum of isopropanol esterified MIL-121
30 wt% of DMC were added as soaking liquid.

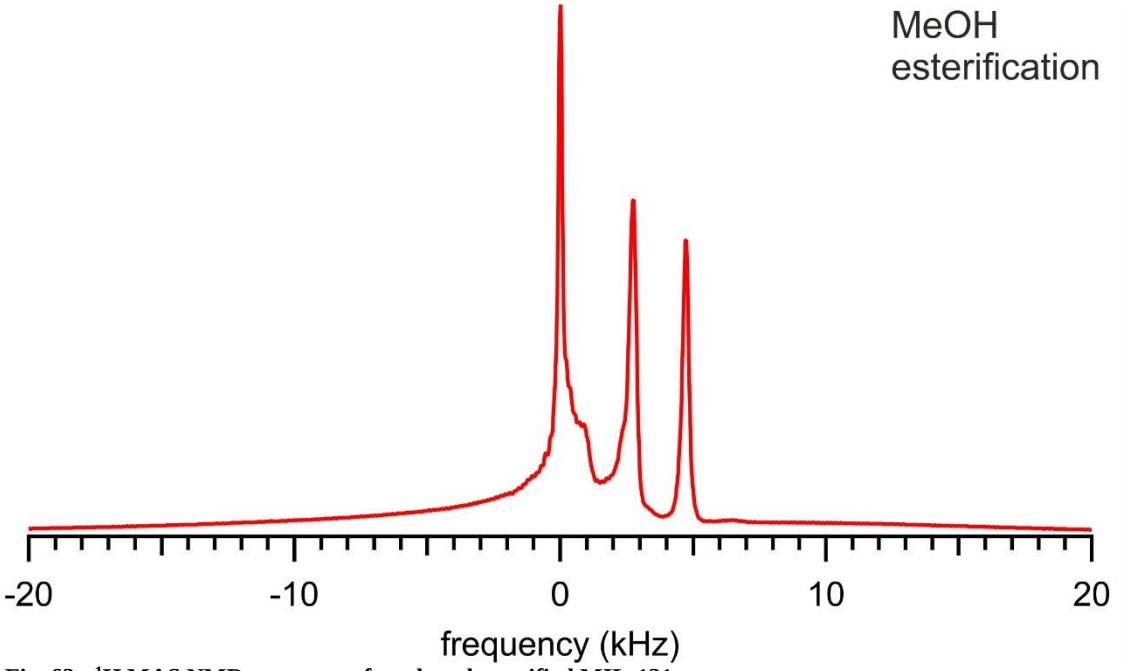

Fig. 63: ^{1}H MAS NMR spectrum of methanol esterified MIL-121

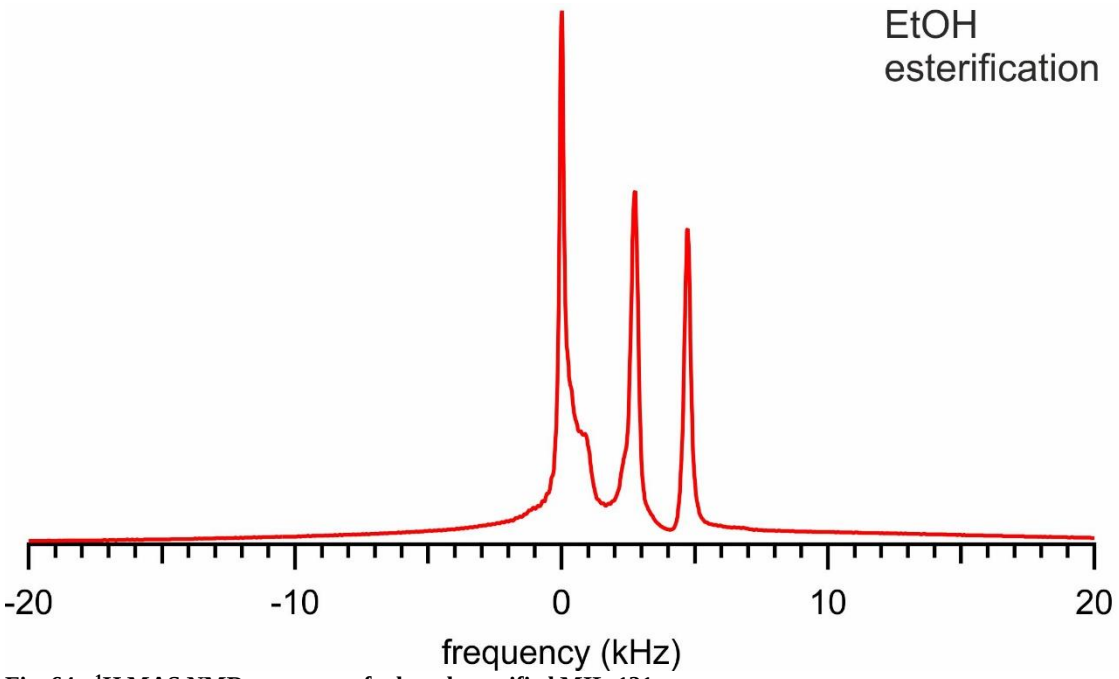

Fig. 64: ^{1}H MAS NMR spectrum of ethanol esterified MIL-121

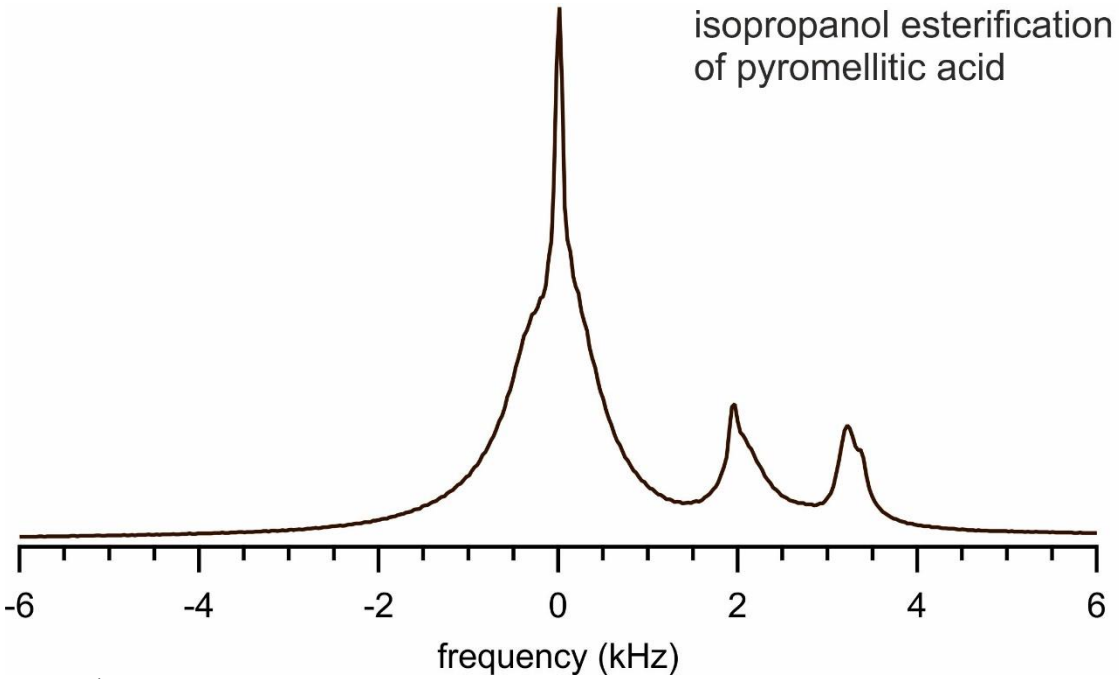

Fig. 65: ^{1}H MAS NMR spectrum of isopropanol esterified pyromellitic acid

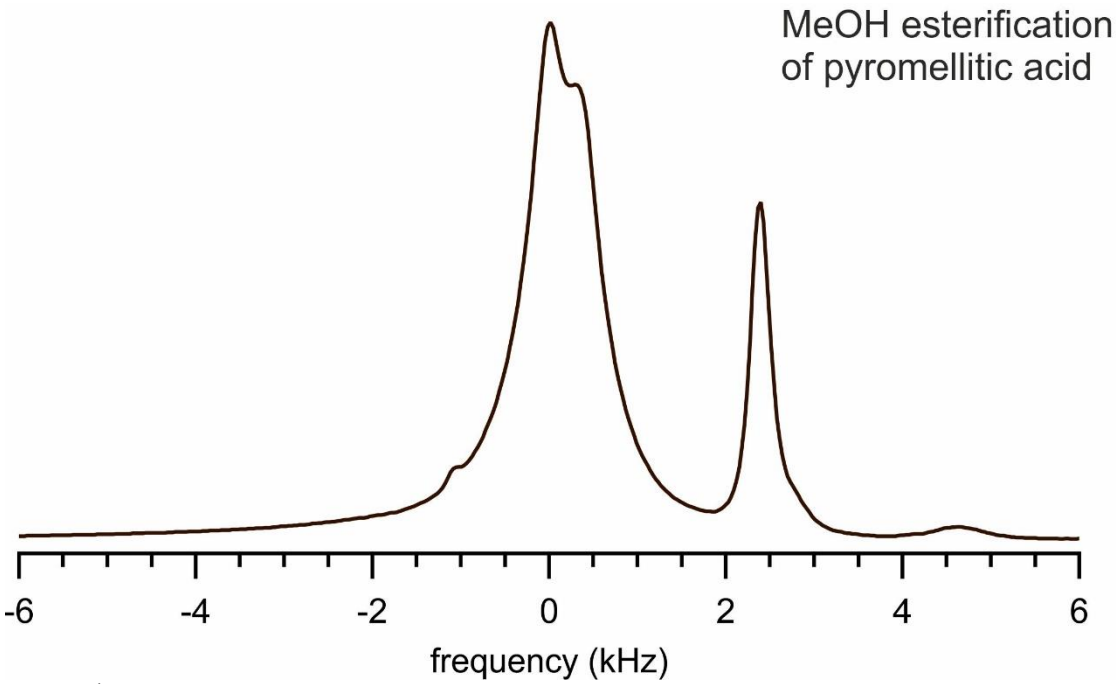

Fig. 66: ^{1}H MAS NMR spectrum of methanol esterified pyromellitic acid

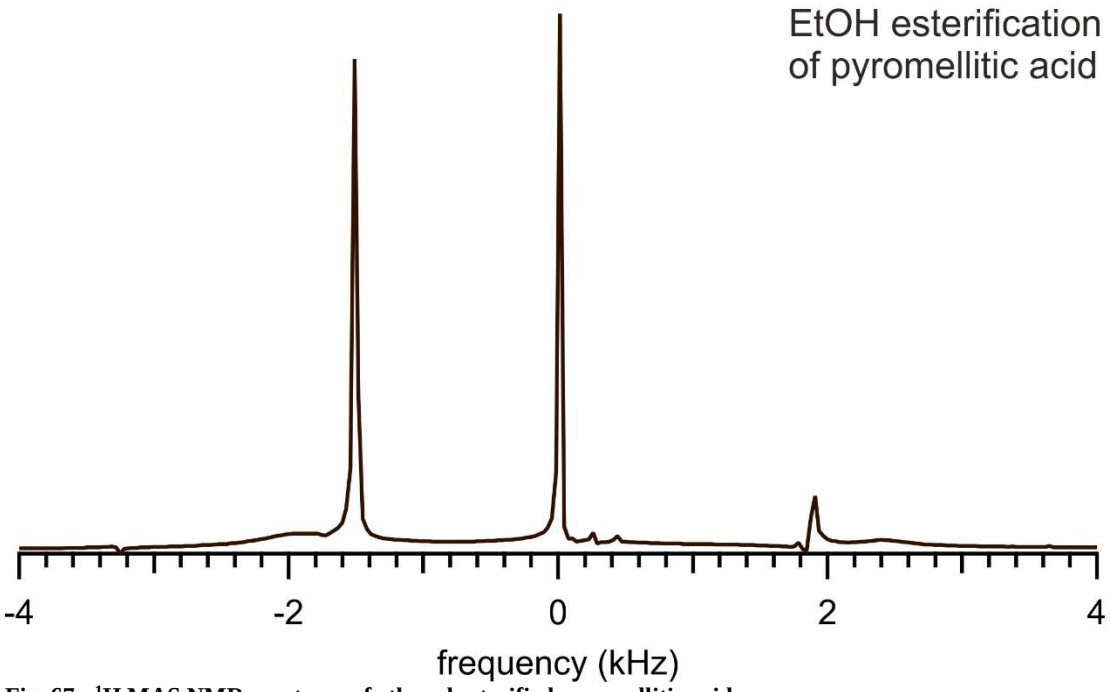

Fig. 67: ^{1}H MAS NMR spectrum of ethanol esterified pyromellitic acid

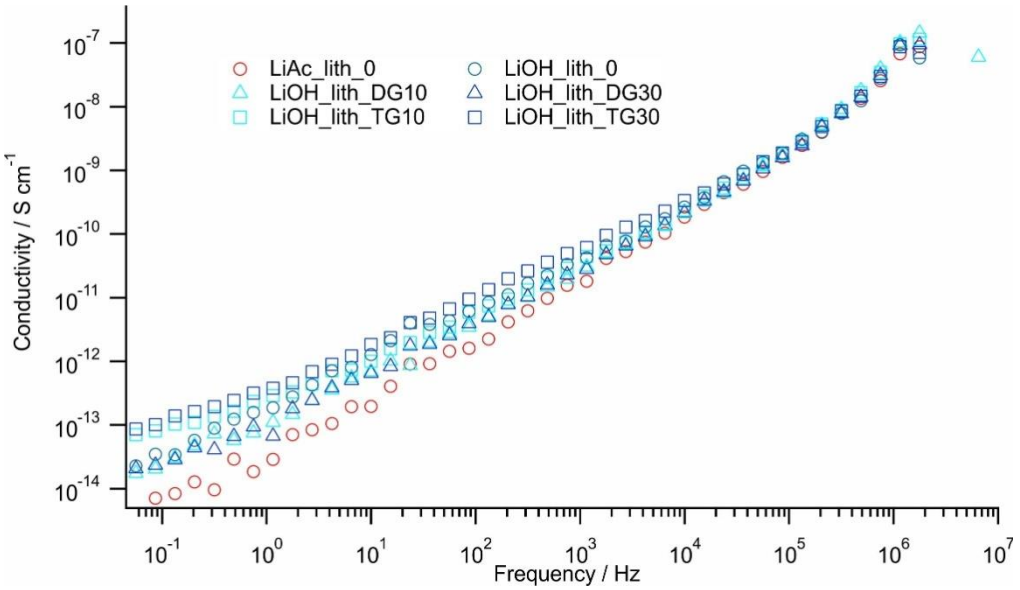

Fig. 68: Conductivity spectrum of LiAc and LiOH lithiation with different amounts of diglyme and tetraglyme added
LiAc…lithium acetate lith…lithiation *e.g.* E10…10 wt% EMIM-TFSI added

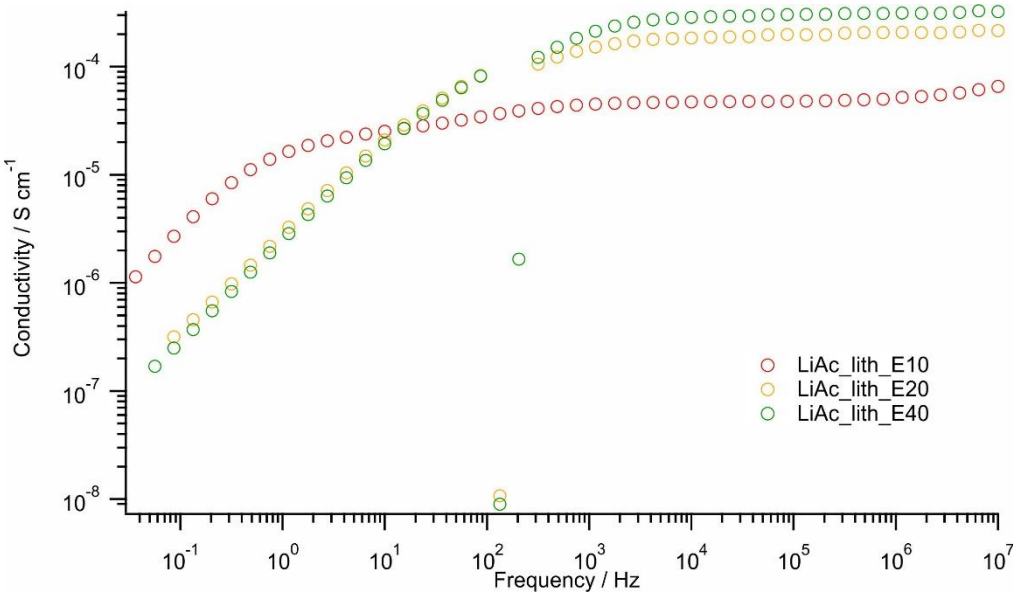

Fig. 69: Conductivity spectrum of LiAc lithiation with different amounts of EMIM-TFSI added
LiAc…lithium acetate lith…lithiation *e.g.* E10…10 wt% EMIM-TFSI added

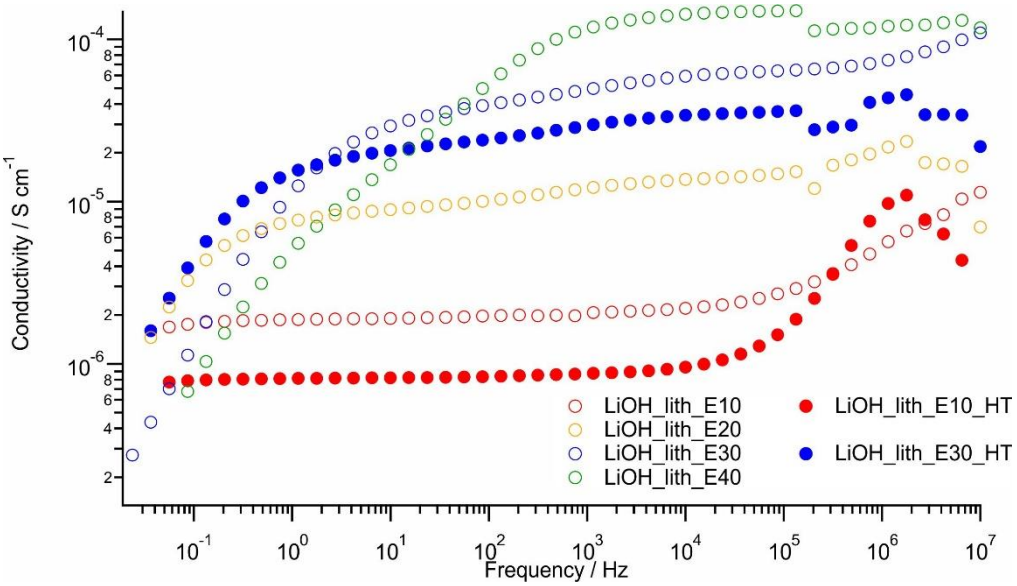

Fig. 70: Conductivity spectrum of LiOH lithiation with different amounts of EMIM-TFSI added as well as a comparison with higher temperature drying (280 °C instead of 220 °C)
LiOH…lithium hydroxide lith…lithiation *e.g.* E10…10 wt% EMIM-TFSI added
HT…high temperature

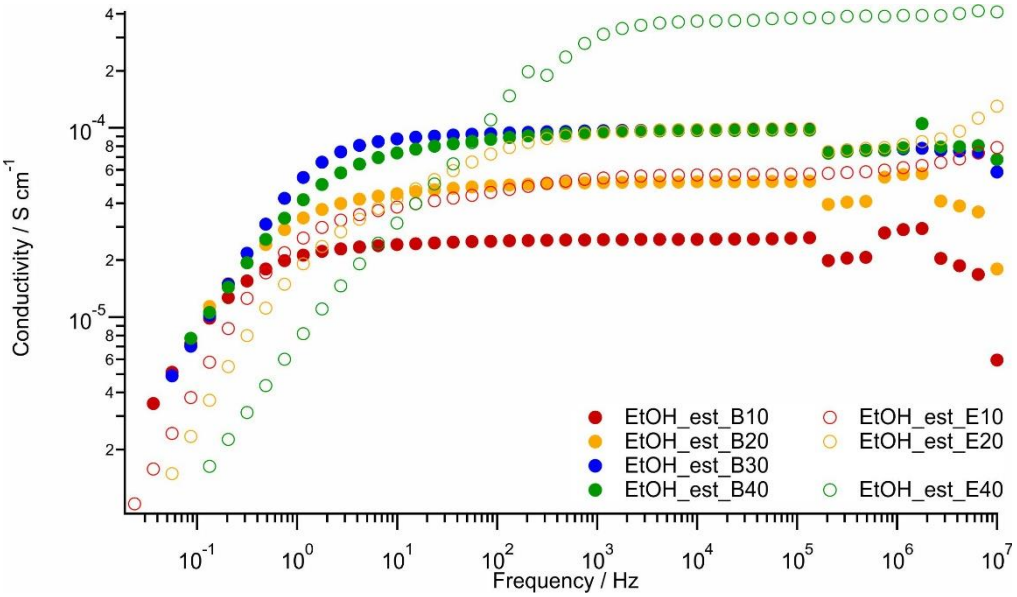

Fig. 71: Conductivity spectrum of EtOH esterification with different amounts of EMIM-TFSI and BMIM-SCN added
EtOH…ethanol est…esterification *e.g.* E10…10 wt% EMIM-TFSI added
e.g. B10…10 wt% BMIM-SCN added

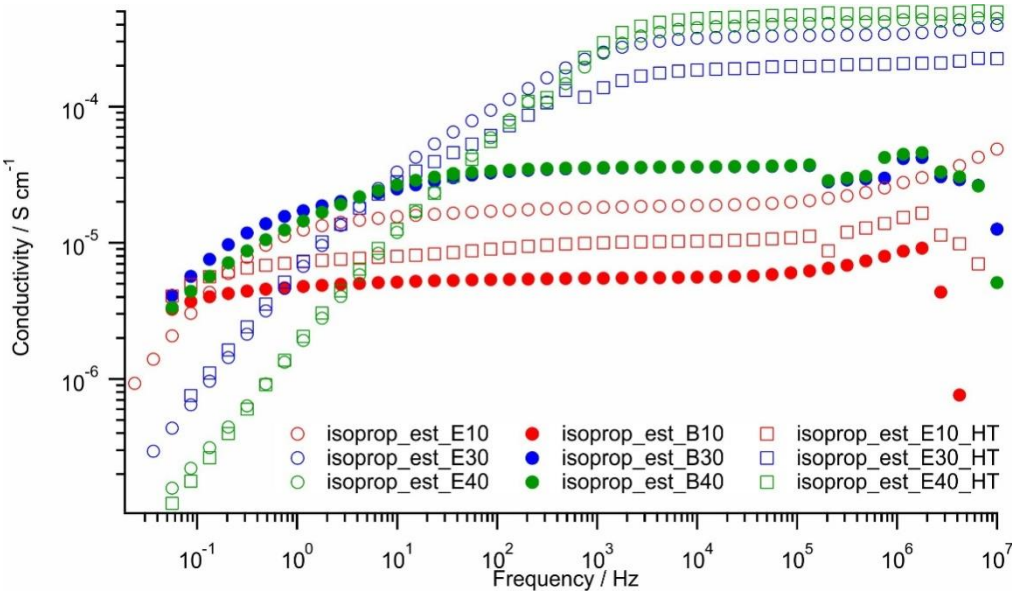

Fig. 72: Conductivity spectrum of isopropanol esterification with different amounts of EMIM-TFSI and BMIM-SCN added as well as a comparison with higher temperature drying (280 °C instead of 165 °C)

isoprop…isopropanol est…esterification *e.g.* E10…10 wt% EMIM-TFSI added
e.g. B10…10 wt% BMIM-SCN added